Magnetic Resonance Imaging 93 (2022) 15–32

Contents lists available at ScienceDirect

Magnetic Resonance Imaging

journal homepage: www.elsevier.com/locate/mri

Review article

# $T_2$ and $T_2$* mapping and weighted imaging in cardiac MRI

Constantin-Cristian Topriceanu [a,b,c], Iain Pierce [a,b], James C. Moon [a,b], Gabriella Captur [a,b,c,d,*]

[a] Cardiac MRI Unit, Barts Heart Centre, West Smithfield, London, UK
[b] UCL Institute of Cardiovascular Science, University College London, London, UK
[c] UCL MRC Unit for Lifelong Health and Ageing, University College London, London, **UK**
[d] The Royal Free Hospital, Centre for Inherited Heart Muscle Conditions, Cardiology Department, Pond Street, Hampstead, London, UK

ARTICLE INFO

*Keywords:*
$T_2$-weighted imaging
$T_2^*$ quantification without mapping
$T_2$ mapping
T2* mapping
Physics
Clinical applications
Future innovations

ABSTRACT

Cardiac imaging is progressing from simple imaging of heart structure and function to techniques visualizing and measuring underlying tissue biological changes that can potentially define disease and therapeutic options.

These techniques exploit underlying tissue magnetic relaxation times: $T_1$, $T_2$ and $T_2$*. Initial weighting methods showed myocardial heterogeneity, detecting regional disease. Current methods are now fully quantitative generating intuitive color maps that do not only expose regionality, but also diffuse changes – meaning that between-scan comparisons can be made to define disease (compared to normal) and to monitor interval change (compared to old scans). $T_1$ is now familiar and used clinically in multiple scenarios, yet some technical challenges remain. $T_2$ is elevated with increased tissue water – edema. Should there also be blood troponin elevation, this edema likely reflects inflammation, a key biological process. $T_2$* falls in the presence of magnetic/paramagnetic materials – practically, this means it measures tissue iron, either after myocardial hemorrhage or in myocardial iron overload.

This review discusses how $T_2$ and $T_2$* imaging work (underlying physics, innovations, dependencies, performance), current and emerging use cases, quality assurance processes for global delivery and future research directions.

## 1. Introduction

Improved myocardial substrate pathology stratification has been a modern research goal as it could lead to earlier diagnoses, better timed and bettter targeted therapy and improved outcomes in patients suffering from heart disease. The pleomorphic myocardial response to insults can result in a variety of pathological manifestations including: inflammation, infiltration, deposition, and fibrosis [1]. Although the gold standard for assessing myocardial pathology remains the direct histological, immunohistochemical and virological analysis following endomyocardial biopsy (EMB), the latter has several limitations: (1) variable yield due to skip lesions, (2) inter-observer intterpretation variability between expert pathologists, (3) paucity of standardized quantifiable pathological markers, and (4) risk of serious complications (e.g., ventricular rupture, arrhythmia, death) [2]. In addition, there are no sufficiently reliable serum biomarkers to quantify: inflammation, infiltration, deposition, and fibrosis [3–6]. Thankfully, noninvasive myocardial tissue characterization is possible using cardiovascular magnetic resonance (CMR) which exploits underlying tissue magnetic relaxation times: $T_1$, $T_2$ and $T_2$* [7].

Initial $T_1$ and $T_2$ weighting imaging methods were only able to highlight regional disease, but the fully quantitative $T_1$ and $T_2$ maps are now able to capture diffuse changes. This opens the prospect of defining disease (compared to health) and monitoring interval change (compared to previous scans). $T_1$ mapping is widely used, and a comprehensive review on it was previously published [8]. The role of $T_2$ and $T_2$* mapping is now also burgeoning in clinical practice with a myriad of prototypes and advances now available. $T_2$ increases with water content, and in the presence of high troponin levels suggests myocardial inflammation. $T_2$* falls in the presence of paramagnetic ions and lower levels suggest a higher myocardial iron content (e.g., iron overload).

The current review summarizes the underlying physics and the spectrum of $T_2$ imaging sequences applicable to cardiology (i.e., $T_2$-weighted imaging [$T_2$WI], $T_2$ mapping, $T_2$* quantification without mapping and $T_2$* mapping) and scrutinizes their clinical utility. In addition, we highlight some recent technical innovations, the need for protocol standardization and conclude with future research directions.

* Corresponding author at: Institute of Cardiovascular Science, University College London, Gower Street, London WC1E 6BT, UK.
*E-mail address:* gabriella.captur@ucl.ac.uk (G. Captur).

https://doi.org/10.1016/j.mri.2022.07.012
Received 7 March 2022; Received in revised form 20 July 2022; Accepted 20 July 2022
Available online 30 July 2022

## 2. Physics and sequences for $T_2$ imaging

Typical scanning protocols for $T_2$WI, $T_2$ mapping, $T_2$* quantification without mapping and $T_2$* mapping have been provided by the Society for CMR, with the most recent update being in 2020 [9]. Table 1 broadly summarizes the strengths and limitations of some key sequence examples.

When a tissue is subjected to a strong magnetic field, the atomic nuclei with non-zero spin (e.g., hydrogen for clinical imaging) behave like tiny rotating magnets and tend to align along the direction of the field [10]. The resulting net magnetization can be disturbed from its resting state by applying a second perpendicular field, rotating at the resonance frequency of the nuclei. For magnetic resonance imaging (MRI), the frequency of this field lies within the radiofrequency range and so is called an RF pulse. When the RF pulse is stopped, the spins relax and return to their resting state [10]. Quantifiable differences in the relaxation times between tissues is one of the core principles of image contrast in MRI [11].

$T_1$ time captures the recovery of longitudinal magnetization (along the strong magnetic field) which is influenced by the chemical environment (it lengthens with edema, fibrosis, and infiltration e.g., amyloid infiltration, but shortens in the presence of fat and iron). Conversely, $T_2$ time measures the decay in transverse magnetization (perpendicular to the strong magnetic field) of tissue that is influenced by how bound or free the spins are. This relates to the water content making it particularly useful at characterizing pathologies causing myocardial edema. As hinted to above, transverse magnetization is the component of the net magnetization in the transverse plane. An RF pulse rotates/tips the net magnetization and the component spins start in phase. Several mechanisms including, spin-spin interactions result in a loss of phase coherence, therefore reducing the net transverse magnetization ($T_2$ relaxation) [10]. Inhomogeneities in the main field, both intrinsic and as a result of susceptibility induced distortions from the tissue (e.g., high content of paramagnetic iron), cause further phase dispersion [12]. The resultant relaxation time is called $T_2$* and it is always less than or equal to the natural $T_2$ on account of $B_0$ inhomogeneities (**Equation 1**) [13]. Although attempts to provide reference ranges for $T_1$ [14,8] and $T_2$ [15,16] times in health and disease have been made, these are usually center and magnet/prototype-specific so not immediately generalizable for widespread use.

MRI pulse sequence modifications generate images with different contrasts [11]. For example: a long TR allows more complete $T_1$ recovery reducing $T_1$ weighting; a longer time-to-echo (TE, i.e., the time between the excitatory RF pulse and receipt of the echo signal) allows increased $T_2$ decay and so increases $T_2$ weighting [11,17]. Local field inhomogeneities lead to bulk dephasing effects which can be eliminated with the application of a 180° refocusing RF pulse [18]. Briefly, a 90° RF pulse tips the spins into the transverse plain [10] and the magnetization dephases in a $T_2$*-dependent fashion (i.e., dependent on T2 and local magnetic field inhomogeneities) [13]. Then, a 180° RF refocuses the spins by reversing dephasing due to the local field inhomogeneities so that the spins are back in phase at the TE after the initial 90° pulse [19]. Thus, sequences such as spin echo (SE) (Fig. 1), contain 180° 'refocusing' RF pulses and generally produce $T_2$-weighted images ($T_2$WI) [19], while sequences which don't (gradient echo, GRE), will be $T_2$*-weighted [20,21].

### 2.1. $T_2$-weighted imaging

Increased water content leads to a longer $T_2$ relaxation time [22]. Thus, $T_2$WI results in a region of hyperintense signal for a qualitative assessment of the presence of edema [23]. $T_2$WI is broadly divided into "dark blood" (DB) and "bright blood" (BB) sequences [18]. SE sequences have some inherent nulling of flowing blood as blood that sees the 90° pulse but not the 180° one, does not contribute to the echo signal [13]. However, much of the imaging is performed during still periods in the cardiac cycle wherein the blood flow is slower. As such, DB $T_2$WI [24] relies on inversion recovery (IR) pulses [25] (Fig. 2) to capture static myocardial anatomy while nulling blood flow signal (i.e., blood flowing inside vessels or cardiac chambers, appears black) [26]. This is commonly used for single shot imaging for anatomical coverage of the thorax such as Half-Fourier Acquisition Single-shot Turbo spin Echo (HASTE) [27] (Table 1). In CMR, conventional $T_2$WI of edema historically used a turbo spin echo (TSE) readout with DB preparation but this method is subject to artifacts such as posterior wall signal loss due to cardiac motion, and bright subendocardial rims due to stagnant blood [28]. Blurring due to cardiac motion can be minimized by using segmented TSE, where data is acquired over multiple heartbeats [18].

Fat remains bright but an additional IR RF pulse can be added to suppress it, in a technique known originally as short-inversion time inversion recovery (STIR)[29], later renamed and commonly referred to as short-*tau* inversion recovery, Fig. 3). Despite these optimizations, DB $T_2$WI techniques are unable to differentiate slow flowing blood from subendocardial edema (as the signal is not suppressed in low flow blood pooling often at the blood-myocardial interface), are limited by motion artifacts of the contracting myocardium especially in arrhythmias and are poor at detecting global myocardial edema [13]. On the other hand, BB $T_2$WI retains the brightness of the blood pool. Fast GRE sequences can be broadly divided into: (a) incoherent in which the residual transverse magnetization is spoiled, and (b) coherent where the residual transverse magnetization is refocused to contribute to the formation of the steady state (Fig. 4) [30]. From the refocused steady-state free precession (SSFP) sequences, the fully refocused or balanced SSFP (bSSFP) has superseded the pre- or post-excitation SSFP variants [31]. bSSFP is least sensitive to motion, can be performed during free-breathing with averaging of single-shot images to improve the signal-to-noise ratio (SNR)[32] and is relatively insensitive to flow compared to other GRE variants [33]. The signal intensity of fully refocused SSFP depends on the $T_2/T_1$ ratio rather than on $T_2$*, so it behaves more like SE than GRE [31]. As the blood $T_2/T_1$ ratio is higher than that of the myocardium, good blood-myocardial contrast is obtained [30]. However, confounding of subendocardial $T_2/T_2$* readouts from the adjacent blood pool can still be problematic [13]. More $T_2$ weighting can be achieved by using longer TEs, but this will introduce increased banding artifacts[12]. However, these are less problematic at 1.5T or 3 T with local shimming [34]. Image contrast can also be introduced by means of preparation pulses, where the magnetization is manipulated before imaging by a series of RF and gradient pulses. $T_2$ preparation consists of a series of non-selective 90° (excitation) and 180° (refocusing) RF pulses which can be varied to change the amount of $T_2$ weighting. Designed to be insensitive to flow and magnetic field inhomogeneities, an iterative Carr-Purcell Malcom-Levit (MLEV) sequence ($90^ox$, $180^ox$, $180^ox$, $-180^ox$, $-180^ox$, $-90^ox$ non-selective RF) [35] is able to suppress the myocardium ($T_2$=45–50ms) leading to signal uniformity which can highlight arterial blood ($T_2$=250ms)[36,37] or the presence of edema[32]. The use of composite pulses (e.g., $180^ox$ is a $90^ox$, $180^ox$, $90^ox$ composite) promotes more uniform off-resonance behavior[38]. By employing $T_2$ preparation before bSSFP (i.e., $T_2$-prepared bSSFP) to promote $T_2$ weighting, shorter TEs can be used to minimize banding artifacts [33]. In addition, the acquisition time will also be smaller which reduces motion blurring from cardiac motion [34].

### 2.2. $T_2$ mapping

To overcome the limitations described above of DB and BB $T_2$WI, the concept of parametric mapping arose. Parametric maps display the pixelwise relaxation time in ms, usually in a color-coded fashion, enabling both the visual identification and quantification of both regional but also diffuse myocardial disease [39].

For $T_2$ mapping, multiple images with increasing $T_2$ weighting are employed to generate a transverse relaxation curve [40]. Data is most commonly acquired as $T_2$-prepared single-shot images, in a single

**Table 1**
Broad comparison of the strengths and limitations of $T_2$WI, $T_2$ mapping, $T_2$* quantification without mapping, and $T_2$* mapping. Further sequences and sequence refinements exist that are not included here.

| | Blood suppression | Sequence category | Example | Sequence description | Imaging pulse sequence | Strengths | Limitations |
|---|---|---|---|---|---|---|---|
| **T-weighted imaging** | Dark blood | Double inversion recovery (IR) [25] | RARE [227] | -Preparatory 180° IR pulse suppresses blood<br>-Multiple echoes within a single repetition time | Fast/turbo spin echo | -Blood flow suppression | -Fat stays bright<br>-Cannot differentiate low blood flow from edema<br>-Limited by motion artifacts<br>-Poor performance in global edema |
| | | | HASTE [27] | -Preparatory 180° IR pulse suppresses blood<br>-Multiple 180° echoes with short inter-echo time<br>-Phase-conjugate symmetry to reconstruct *k*-space by acquiring half of it | | | |
| | | Triple inversion recovery [228] | STIR [25,29] | -Preparatory 180° IR pulse suppresses fat<br>-Additional preparatory 180° IR pulse suppresses blood | Segmented fast spin echo | -Blood flow suppression<br>-Uniform fat suppression<br>-Relatively insensitive to $B_0$ or presence of metals<br>-Additive $T_1$ and $T_2$ contrasts | -Cannot differentiate low blood flow from edema<br>-Arrythmias can cause signal inhomogeneities concealing edema<br>-Limited by motion artifacts<br>-Poor performance in global edema |
| | Bright blood | Spoiled-gradient echo [20] | FLASH [229]/ SPGR/ RSSG | -Spoiler RF pulse eliminates any transverse magnetization after each pulse | RF-spoiled gradient echo | - No streaking artifact due to $T_2$* effects | -Spin clustering and cycle-related spoiling variability may create bias |
| | | Pre-excitation Refocused SSFP [33] | SSFP/ Reversed FISP/ TRSG/ $T_2$-FFE | -Rewind gradient rephases $T_2$* magnetization pre-excitation | Partially refocused gradient echo | -Preserve $T_2$* effects enabling detection of calcification and hemorrhage | -Sensitive to $B_0$ due to magnetic tissue susceptibilities (e.g., blood-myocardium interface) reducing SNR<br>-Subendocardial confounding<br>-Blood-sensitivity to motion artifacts |
| | | Post-excitation refocused SSFP [33] | GRASS/ FIST/ FFE | -Rewind gradient rephases the $T_2$* magnetization post-excitation | Partially refocused gradient echo | | |
| | | Fully refocused SSFP [31] | True FISP [230]/ FIESTA/ Balanced FFE/ True SSFP | - RF pulses alternating between 0° and 180° are applied to refocus all gradients | Balanced fully refocused gradient echo | -Least sensitive to motion artifacts<br>-Relatively insensitive to blood flow<br>- Good blood-myocardial contrast<br>-High SNR<br>-Detects calcification and hemorrhage | -Banding artifacts<br>-Subendocardial confounding of low blood flow with edema |
| **$T_2$mapping** | Dark blood | Double inversion recovery with $T_2$-prepared SSFP [51] | BEATS [51] | -Starts with a non-selective RF pulse with heart rate adaptive flip angle to ensure blood suppression within a RR interval<br>-180° IR pulse suppresses blood<br>-Single-shot SSFP readouts | Refocused gradient echo | -Good visualization of blood-myocardial interface<br>-Able to detect subendocardial edema | -Limited number of slices acquired per scan<br>-Artefact prone in dyskinetic myocardial regions |
| | Bright blood | Spin echo | Single-shot TSE [231] | -Multiple 180° echoes with short inter-echo time echoes<br>-Acquires all *k*-space within a 90° excitation pulse | Turbo spin echo | -Rapid acquisition<br>-Good SNR as longer TR allows more time for recover<br>-Good contrast due to more phase-encoding lines<br>- Low susceptibility to ghosting artifacts | -Motion artifacts because of long Acquisition windows<br>-Blood flow artifacts at the blood-myocardial interface<br>-Misses hemorrhage and calcification |
| | | Gradient spin echo | GraSE [232] [233] | -Train of spin echoes generated within each RR-interval using ECG-gating<br>-GRE EPI for readouts | Spin echo and gradient echo | -hemorrhage and calcifications<br>-Fewer artifacts at tissue interfaces compared to TSE | -EPI readouts can underestimate $T_2$ as $T_2$* effects are introduced<br>-Can underestimate $T_2$ because of $B_0$ |

(*continued on next page*)

**Table 1** (*continued*)

| | Blood suppression | Sequence category | Example | Sequence description | Imaging pulse sequence | Strengths | Limitations |
|---|---|---|---|---|---|---|---|
| | | | | | | | -As the readout occurs in different phases of the cardiac cycle, $T_2$ values can be slightly biased<br>-Unreliable for subendocardial edema |
| | | $T_2$-prepared SSFP [32] | True FISP/ FIESTA/ Balanced FFE/ True SSFP | -$T_2$-preparatory phase (usually SE sequence to generate $T_2$ contrast)<br>-Single-shot SSFP readouts | Refocused gradient echo | -Highly reproducible<br>-More accurate<br>-Less prone to motion artifacts compared to the other bright blood techniques | -$T_2$ may be overestimated as the SSFP readout can introduce mixed $T_1/T_2$ contrast<br>-Subendocardial confounding of low blood flow with edema |
| **$T_2^*$quantification without mapping** | Dark blood | Double inversion recovery [52] | - | -R-wave triggered double inversion pulses with inversion time extended into diastole | Multi-gradient echo | -Improved image contrast compared to bright blood<br>-Reduced epicardial artifacts arising from great cardiac veins<br>-Better $T_2$* decay curve fitting<br>-Superior intra- and inter-observer reproducibility in transfusion-related conditions | -Susceptible to motion artifacts<br>-Variable reproducibility compared to $T_2$* mapping<br>-Confounding epicardially and subendocardially from the deoxygenated blood |
| | Bright blood | Multigradient echo [52] | FFE | -Multi-gradient echo acquires images at different echo times<br>-Very short repetition times and small flip angles of the excitation pulses for fast image acquisition | Multi-gradient echo | -Acceptable visual detection of myocardial areas with increased iron | -Acquisition time is heart rate dependent<br>-More susceptible to heart motion artifacts<br>-More likely to overestimate the myocardial iron content<br>-Epicardial artifacts related to the great cardiac veins |
| | | | GRE EPI [64] | -Multi-gradient echo is employed to acquire images at different echo times<br>-Single-shot EPI is then used to cover the entire k-space | Multi-gradient echo | | |
| **$T_2^*$mapping** | Dark blood | Double inversion recovery [52] | Same as in **$T_2^*$ quantification without mapping** | | Multi-gradient echo | Compared to $T_2$*quantification without mapping:<br>-Objective detection and quantification of myocardial iron<br>-Increased reproducibility especially with automated LV segmentation<br>-Reduced susceptibility to motion artifacts<br>-Improved contrast especially in pixelwise generated $T_2$* maps | -$T_2$* decay curve plateaus at long TEs and current truncation methods are imperfect<br>-Inability to detect fibrosis requiring $T_1$ mapping and ECV estimation to provide complementary data to aid in the understanding of the myocardial effects of iron deposition |
| | Bright blood | Multigradient echo [52] | | | Multi-gradient echo | | |

*BEATS = black blood heart-rate adaptive $T_2$-prepared balanced SSFP; ECV = extracellular volume; FISP = fast imaging with steady state precession; FLASH = fast low angle shot; GraSE = gradient spin echo; GRE EPI = gradient echo echo-planar-imaging; GRASS = gradient-recalled acquisition in the steady state; HASTE = half-Fourier acquisition single-shot turbo spin echo; IR = inversion recovery; RARE = rapid acquisition with relaxation enhancement; RSSG = radio-frequency spoiled SARGE; SARGE = steady-state acquisition rewound gradient echo; SPGR = spoiled gradient-recalled; SSFP = steady-state free precession; SSFP = steady-state free precession; STIR = short tau inversion recovery; $T_2$-FFE = $T_2$fast field echo TRSG = time-reversed SARGE; TSE = turbo spin echo; WI = weighted imaging.*

breath-hold over multiple electrocardiogram (ECG) RR intervals with motion correction applied [41]. An alternative to single shot imaging is to acquire multiple segmented images from different breath-holds with different TEs followed by post-processing which includes map co-registration, but the latter can be problematic given the slightly different breath-hold positions [42]. Thus, single-shot imaging bypasses the map co-registration issue, and is faster to acquire, but the spatial resolution is reduced [41]. A TR ranging from 2–4 RR intervals is used to allow sufficient $T_1$ recovery, reducing $T_1$ influence, otherwise $T_2$ map distortion can result [41]. Like $T_2$WI, $T_2$ mapping can be achieved using BB sequences such as TSE [43,44], multi-echo spin echo (MESE)[45], gradient spin echo[46] (GraSE), or $T_2$-prepared bSSFP [39] which is the commonest method used in clinical practice since it has showed a greater accuracy compared to other methods [41], is less prone to artifacts and flow related signal loss [34] and is highly reproducible [47] (Table 1). The latter starts with a $T_2$-preparatory phase employed to

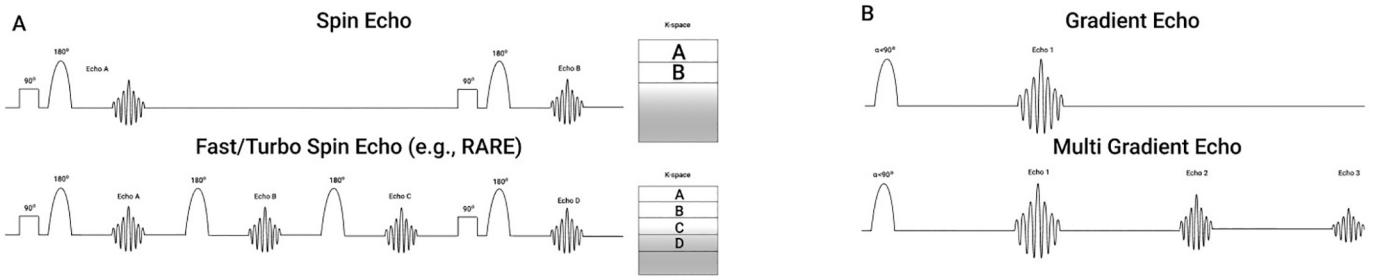


**Fig. 1.** Simplified comparison of spin echo *vs.* fast/turbo spin echo vs gradient echo vs multi-echo gradient echo.
**A.** If a tissue is excited by a radiofrequency (RF) pulse, the measured transverse magnetization reduces in a process called free induction decay (FID) [21]. If a second RF pulse is applied before FID is complete, some of the measured transverse magnetization is recovered as the spins are re-focused – a process called a spin echo (SE) [19]. The classical SE sequence (top image) consist of a 90° RF pulse to tip the net magnetization from the *z*-axis to the transverse (xy) plane, followed by 180° RF pulse (at half of the time to echo [TE]) to refocus phase incoherence due to $B_0$ inhomogeneities (19). Thus, the decay in transverse magnetization can be quantified. This is due to $T_2$ and $T_1$, but mainly $T_1$ as for these tissues $T_2$ is much smaller than $T_1$ [234]. Further 180° RF pulses can be used with similar timing around the echo to produce a train of echoes, and phase encoding gradients can be stepped between the echoes to collect multiple lines of *k*-space in the same repetition time (TR) [27,227].
The increased time efficiency of the fast/turbo SE (FSE/TSE)sequence allows: (1) shorter acquisition times for the same image; (2) increased recovery time between 90° RF excitations; and (3) increased resolution in a similar acquisition time [235]. However, it over-amplifies the brightness in already bright tissues such as fat which is thought to occur due to the disruption of J-coupling interactions between adjacent (fat) protons [236].
**B.** In gradient echo (GRE) imaging, gradient fields are used to generate transverse magnetization (not shown) and the flip angle is usually less than 90° [237]. By repeating the gradient reversal process multiple GREs which temporally decrease in intensity can be produced following a single RF pulse [20].
FID= free induction decay; FSE= fast spin echo; GRE= gradient echo; RF = radiogrequency; SE= spin-echo; TE= time to echo; TR= repetition time; TSE= turbo spin-echo.

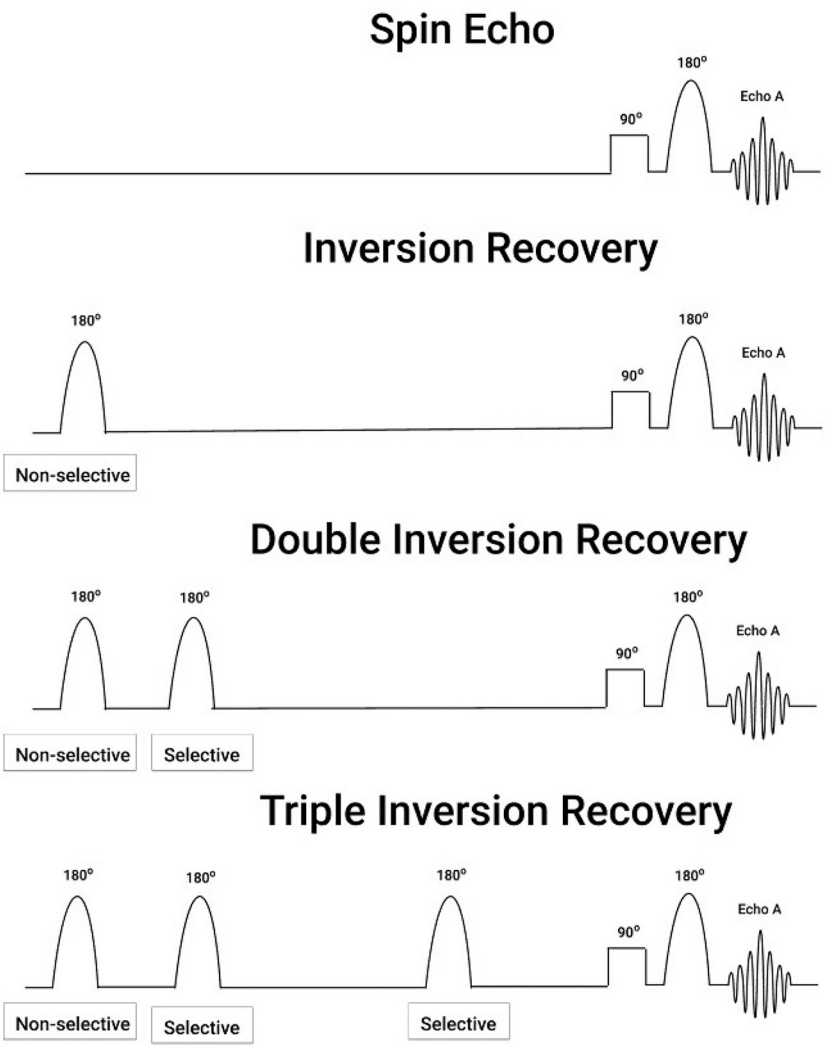


**Fig. 2.** Generic summary of inversion recovery sequences.
**A**. A SE sequence (without any inversion recovery [IR]) is shown[19].
**B.** A simple IR sequence (2nd row) starts with a 180° RF pulse followed by a SE module (top row, 90° RF pulse + 180° RF pulse, and see Fig. 1) [24]. An inversion pulse can be timed with a delay before imaging such that the blood signal is passing through the null point and so will give no signal [25]. However, relatively small differences between blood and muscle $T_1$ would mean that muscle signal is very low. Thus, a simple IR would black out most of the myocardium [26].
**C.** A double IR (DIR) sequence needs to be employed (3rd row). A 2nd IR pulse can also be applied immediately after the 1st to reinvert/recover all the signal within the imaged slice (and hence it is slice-specific), imaging then occurs when blood signal from outside the slice is passing through the null point and has replaced the blood that was in the slice during the second inversion pulse [26]. Any blood flowing into the slice after this time would have a black signal, but the myocardium would not be nulled [26].
**D.** Triple IR (TIR, bottom row) employs an additional 3rd slice-selective 180° RF pulse prior to image acquisition to null fat [25,228]. Note that the inversion time (TI) to null blood is higher in TIR than DIR as the 3rd IR pulse re-inverts the magnetization of blood which should reach zero before the acquisition stage [228]. The ideal TIs are often hard to achieve with the common heart rates. Thus, this is one of the causes of artifacts in STIR-T2 TSE imaging [29]. Please note that the DIR pulses (not to scale) are applied in close succession with minimal delay. DIR = double inverstion recovery; IR = inversion recovery; STIR = short tau inversion recovery; TI = inverstion time; TIR = triple inversion recovery. Other abbreviations as in Fig. 1.

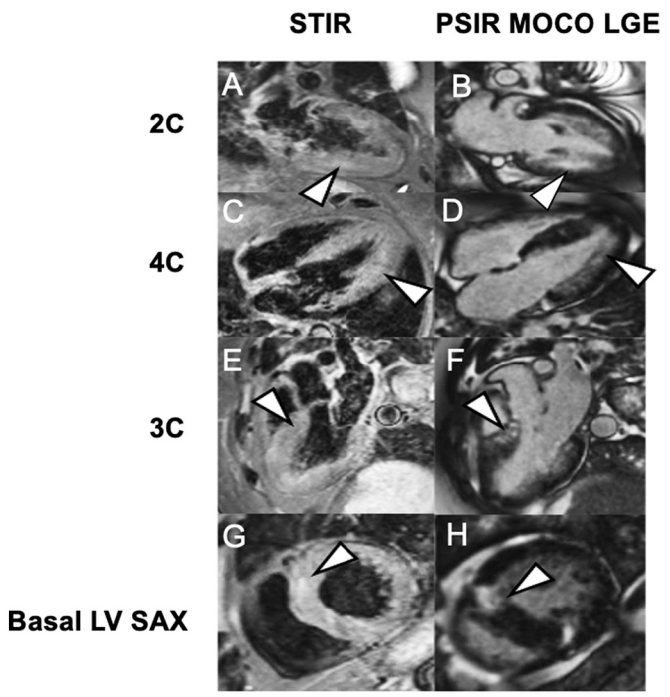


**Fig. 3.** The role of STIR imaging in identifying myocardial edema in the inflammatory phase of hypertrophic cardiomyopathy.
2Ch (**A, B**), 4Ch (**C, D**), 3Ch (**E, F**) and basal LV SAX (**G, H**) views showing extensive non-infarct pattern LGE in multiple myocardial segments with matching hyper-intense signal on STIR suggestive of myocardial edema.
Ch = chamber; LV = left ventricle; LGE = late gadolinium enhancement; MOCO = motion-corrected; PSIR = phase-sensitive inversion recovery; SAX= short-axis, STIR = short tau inversion recovery.

generate $T_2$ weighted contrast [31]. Then, a spoiler gradient is usually employed to remove any residual transverse magnetization which is followed by a bSSFP readout (Fig. 4) [48]. $T_2$ maps are generated following a voxel-wise 2-parameter model fit for relaxation based on multiple $T_2$-prepared bSSFP images [39,49]. $T_2$-prepared bSSFP-based $T_2$ mapping has several SSFP advantages as described above, but it has an inherent $T_1$ bias related to the variable signal decay after the preparatory phase [50]. For example, when the myocardial $T_1$ is short (e.g., Fabry's disease [FD]), $T_2$ times tend to be overestimated. The opposite holds when myocardial $T_1$ times are long (e.g., amyloidosis) [33].

DB $T_2$ mapping is more challenging as the IR sequences are not readily applicable. There have been attempts using DB $T_2$-prepared SSFP such as black blood heart-rate adaptive $T_2$-prepared balanced steady-state free-precession (BEATS)[51], but they are limited mainly by acquisition time as usually 1 slice is acquired per scan.

### 2.3. $T_2$* quantification without mapping and $T_2$* mapping

Essentially, $T_2$* time captures the decay in transverse magnetization due to the combined effect of $B_0$ field inhomogeneities and spins dephasing [13]. As $T_2$* is extremely sensitive to $B_0$ field inhomogeneities which are higher at 3T compared to 1.5T, $T_2$* maps are classically acquired clinically at 1.5T, although attempted usage at higher field strengths in research settings is steadily increasing [52]. $T_2$* quantification is done using gradient echo imaging with multiple echoes being acquired after each RF excitation pulse until there is a complete loss of the transverse magnetization (multi-echo GRE) [53]. The gradients for the next echo can be used to rewind the phase from the previous echo with each subsequent echo being smaller than last one [33]. Then, measurements are made in regions of interest (ROI) and curve fitting is applied to quantify the $T_2$* [54]. The $T_2$*WI could be either BB acquired in diastole (i.e., immediately after the R-wave when ECG-gating) to limit motion artifacts [52] or DB which involve a DIR pulse to nullify blood signal. While BB sequences fell out of favor early on because of their tendency to overestimate myocardial iron and because of their susceptibility to epicardial artifacts, DB sequences offered better image quality, better $T_2$* curve fitting, and better reproducibility in transfusion-dependent conditions such as thalassemia [55]. Mainly this is thanks to the elimination of the blood signal which otherwise creates partial volume effects, contaminating pixels at the blood-myocardial interface. DB sequences can also reduce magnetic susceptibility effects on the myocardium arising from deoxygenated blood in cardiac veins [52].

In $T_2$* quantification without mapping, ROIs are applied across all different TE images and the signal is plotted against time followed by exponential fitting [52]. The main difficulties with this stem from the post-processing steps required for $T_2$* calculation. Various methods have been proposed to deal with the signal plateau: (1) truncation: plateau is discarded and the remaining data points are plotted with an exponential equation, or (2) offset: a constant is added to the exponential equation [56]. The main difference between $T_2$* quantification without mapping and $T_2$* mapping is that the latter also outputs a visual parametric map of $T_2$* times in a color-coded fashion, to facilitate interpretation of findings. As mapping simultaneously enables visual identification and quantification allowing both regional and diffuse myocardial disease to be identified, this added feature in $T_2$* mapping has gained a lot of traction. However, not all centers have such added mapping capability, so $T_2$* quantification without mapping still remains the most commonly used prototype in clinical practice globally for measuring myocardial iron deposition.

$T_2$* maps are also generated using a $T_2$* relaxation curve plotted using multiple GRE images collected at different TEs (i.e., a multi-gradient echo [MGE] image series) [57]. The $T_2$* quantification can be done by: (1) ROI averaging of signal intensity on each MGE image in the series followed by $T_2$* relaxation curve fitting, or (2) pixelwise fitting of the signal intensity on each pixel in the ROI of the MGE image series separately, and then reporting the average of the calculated $T_2$* in each pixel [52]. The latter is more accurate [58] and has a better reproducibility [59]. To avoid observer dependence and reduce the analysis time and variability, the ROIs should be automatically generated using automatic LV segmentation which is commonly done via image thresholding [60] or Hough transformation[61].However, this is not the norm yet as the commonest practice is to manually draw a ROI, usually over the mid septum. Pixelwise fitting can be further improved by $R^2$ [62] and SNR ratio[63] truncation fitting to compensate for the signal plateau at longer TEs. Another important topic in the field of $T_2$* mapping is breath hold vs. free breathing techniques [52]. Although breath holding eliminate the problem of respiratory movement artifacts, it puts a time constraint on data acquisition meaning the acquired images are more likely to be noisy which in turn leads to reduced spatial resolution [56]. Thus, free breathing $T_2$* mapping based on highly accelerated GRE [53] or single-shot GRE echo-planar imaging [64] are being explored for their ability to deliver good SNR images in spite of respiratory motions. Lastly, the reciprocal of $T_2$*, called $R_2$* (i.e., $1/T_2$*, measured in Hertz) is another means of displaying the $T_2$* map for hyperintense high iron [53] and reflects the paramagnetism of the tissue [65]. The presence of fat might lead to errors when estimating $T_2$* due to the chemical shift of fat leading to both constructive and destructive inferences [66]. Thus, an alternative to calculate the myocardial $R_2$* is to use the Dixon sequence which can achieve uniform and robust fat suppression, is fast and can be acquired in a single breath-hold making it less prone to motion artifacts [67]. The original two-point chemical shift technique relies on the averaging of two SE acquired at different echo times with water and fat being in-phase and out-of-phase respectively [68]. A multiecho acquisition using Dixon technique can simultaneously achieve fat suppression and estimate both $T_2$* and $R_2$* ($1/T_2$*) [66].

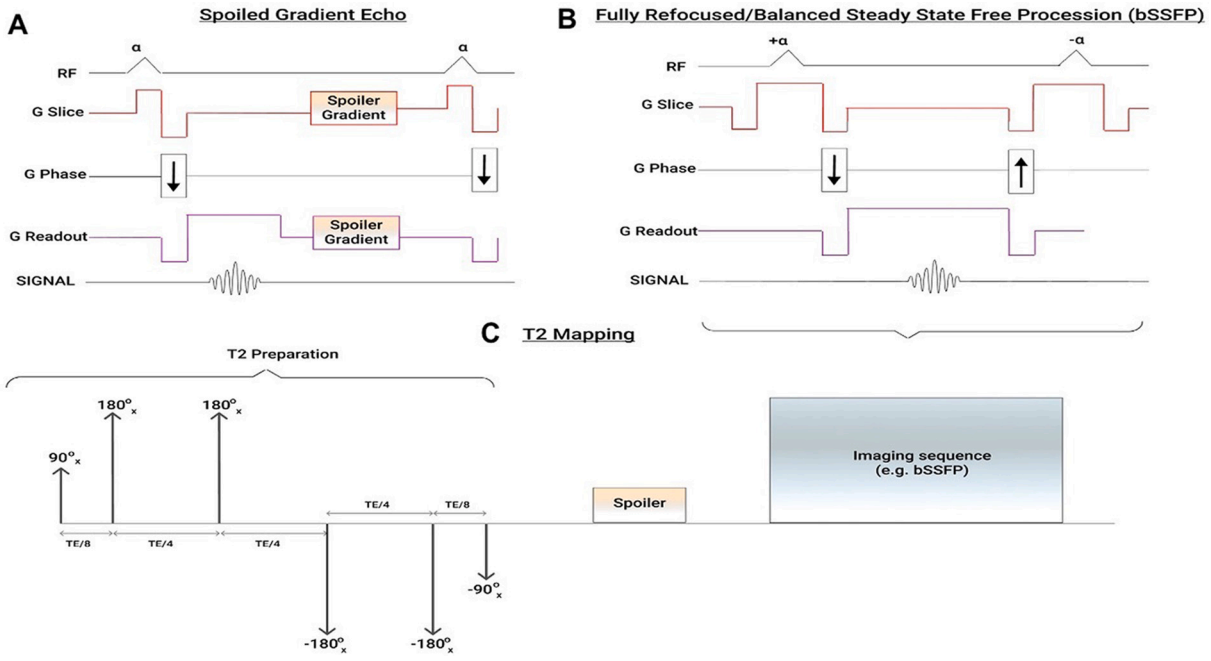


**Fig. 4.** Generic summary of steady-state gradient echo sequences.
In a GRE sequence, the tissue is excited with a $\alpha<90^{o}$ RF pulse [237]. Then, a dephasing gradient accelerates the FID of the magnetized tissue. A rephasing gradient (with an equal moment as assessed by the area under the gradient-time plot) then reverses the FID creating a GRE [20]. As the repetition time is shorter than the $T_2$, there isn't enough time for the residual magnetization to decay before the next radiofrequency pulse [13]. Thus, it can be either spoiled or refocused to achieve a steady state.
**A.** In spoiled GRE, RF spoiling and gradient spoiling are often used in combination [13]. RF spoiling cycles the phase of the RF excitation pulse such that any unwanted future echoes that may form are at such a time after the original pulse that they have very little signal [229]. Gradient spoiling uses large gradient pulses to put in so much phase incoherence that there is no signal recoverable.
**B.** In fully refocused steady state free precession (SSFP) also known as balanced SSFP (bSSFP), gradients are balanced across slice-selection, phase-encoding and readout gradients meaning there is no net magnetization dephasing due to the gradients within the repetition time [48].
**C.** A $T_2$-preparatory phase can be employed to generate $T_2$ contrast (e.g., Carr-Purcell Malcom-Levit sequence [35] as above), followed by a spoiler gradient to remove any residual transverse magnetization [48] and an imaging sequence (usually bSSFP [31] or less commonly GRE) [20] is lastly used for readout. This is commonly used for $T_2$-prepared bSSFP and, with different $T_2$ weightings, for $T_2$ mapping. bSSFP = balanced steady state free precession; SSFP = steady state free precession. Other abbreviations as in Fig. 1.

### 2.4. $T_1$-weighted imaging and mapping

We previously published a comprehensive review on $T_1$ mapping [8], but will briefly provide an overview of the topic. Native $T_1$ captures proton spin-lattice relaxation, and it becomes longer in interstitial expansion (e.g., edema, fibrosis, and infiltration). Measuring native and post-gadolinium contrast agent (PGCA) $T_1$ and correcting for hematocrit forms the basis of extracellular volume (ECV) estimation [69]. Broadly speaking, $T_1$ mapping acquisition is done using inversion recovery preparation as in Modified Look-Locker Inversion Recovery (MOLLI) [70], saturation recovery preparation such as in Saturation Recovery Single Shot Acquisition (SASHA)[71] or both as in Saturation Pulse Prepared Heart-Rate Independent Inversion Recovery Sequence (SAPPHIRE)[72]. 3-Parameter fit SASHA is independent of heart rate [73], not sensitive to $T_2$ [71], less sensitive to imperfect adiabatic inversion [71] and less sensitive to magnetization transfer [74], while MOLLI provides a better dynamic range [8], is less sensitive to artifacts [75] and has a better reproducibility[75]. In spite of the several available $T_1$ mapping sequences, limitations include: susceptibility to off resonance banding effects [76], low spatial resolution at blood-myocardial and myocardial-fat boundaries due to through plane effects [75], and susceptibility to contrast intercompartmental exchange which induces errors in calculated ECVs [77].

## 3. Standardization and quality assurance

$T_2$ and $T_2$* may be affected by age (higher $T_2/T_2$* values in those who were younger) [78,79], sex (lower $T_2/T_2$* values in males) [78–80], $T_2$ mapping sequence (e.g., lower $T_2$ values in $T_2$-prep bSSFP compared to GRASE) [45], field strength (higher $T_2$ values at 1.5 T vs 3 T) [45], myocardial position and segment (e.g., higher $T_2$ values in the apical compared to basal segments) [45,80], and heart rate (higher $T_2$ values at smaller heart rates) [79]. $T_2$ mapping has been established for about a decade, but its widespread implementation in clinical practice is currently hampered by a lack of protocol standardization, use of multiple platforms, sequences and prototypes, and the lack of normal values which makes it difficult to establish cut offs between physiological and pathological states, monitor interval change, pool data from different CMR centers, or conduct high-quality longitudinal studies without the risk of bias. The Society for CMR (SCMR) has urged multicenter studies to perform a stratified statistical analysis as a means of adjusting for each site's scan characteristics [69]. There have been attempts to create age and sex corrected normal values for $T_2$ and $T_2$* [78,81,82], but none are widely accepted. In contrast, an internationally accepted $T_2$ mapping standard would facilitate accurate and reproducible results regardless of scan properties or location in much the same way that the international normalized ratio (INR) for warfarin dosing is universally interpretable regardless of which laboratory has performed the test [83].

The quality assurance field is more advanced for $T_1$ mapping as a robust quality assurance phantom has been in circulation for the past 6 years [84] and has since been extensively validated. However, our research group has recently developed a $T_2$ mapping phantom which will be soon made available to the CMR community [85]. It is also important to note that *in vivo*, 1 standard deviation (SD) of the mean

native myocardial $T_1$ is ~30ms at 1.5 T and ~50ms at 3 T [84], while 1SD of the mean native myocardial $T_2$ is ~ 5ms [86].

## 4. Innovative sequences on the horizon

$T_2$ mapping most commonly relies on acquiring bSSFP after a $T_2$ preparation pulse with varying echo times. To acquire quantitative $T_2$ maps, a TR of 2–4 heartbeats is needed to allow sufficient $T_1$ recovery. This would reduce $T_1$ influence reducing the risk of $T_2$ map distortion [41]. The disadvantage of this approach is that it reduces acquisition efficiency and may underestimate $T_2$ values in tachycardic patients [87] (a particular problem clinically). Potential solutions include: (1) acquiring data in skip counting heartbeats [88], (2) using a saturation pulse before the $T_2$ preparation pulse [89] and (3) combining slice-selective $T_2$ preparation pulses with interleaved slice acquisition with a period of seconds rather than heart beats being used between the images [90]. The latter not only decreases acquisition time four-fold, but also increases spatial coverage.

With the emergence of $T_2$ mapping, there was a research focus shift away from $T_2$WI. However, there have been recent $T_2$WI developments as well, such as 3D fast-spin echo STIR $T_2$W I[91]. A $T_2$WI STIR can suppress both blood flow and fat but since it relies on a stack of short axis sections (8mm with 2mm gap) it cannot fully capture all the intricate details of the LV myocardial thickness which limits its clinical use [92,93]. In contrast, ECG-triggered breath-hold 3D STIR sequences covering the entire left ventricle do not suffer from any acquisition gaps and were superior to $T_1$ and $T_2$ mapping in assessing edema in myocarditis (especially if patchy or regional) [91]. Although DB $T_2$ mapping is still in development and not in mainstream clinical use, BEATS is an exciting prospect as the partial volume effects at the blood-myocardial interface can result in an elevated $T_2$ at the blood-myocardial boundary resulting in its sharper definition [51].

Other innovations have focused on shortening the acquisition time for $T_2$ mapping which is done mostly through k-space under-sampling and image reconstruction and/or signal sharing. Notable proposed methods include: (1) iteratively fitting the decay curve using the Projection onto Convex Sets (POCS) algorithm [94]; (2) simultaneous estimation of spin-density and $T_2$ as the solution of a nonlinear inverse problem [95]; (3) Shared K-space Radial $T_2$ characterization of the Heart (SKRATCH) using accelerated and k-space-weighted image contrast (KWIC)-filtered $T_2$ mapping in which the periphery of the k-space is shared between images with the same geometry [96,97]; (4) free breathing 3D $T_2$ mapping using multiple differentially $T_2$-weighted volumes to acquire voxel-by-voxel parametric maps [89]; (5) combining a 3D motion-corrected under-sampled signal matched (MUST) $T_2$-prepared Cartesian acquisition with high-order patch acquisition (3D MUST-$T_2$ mapping) [98]; (6) model-based accelerated relaxometry by iterative nonlinear inversion (MARTINI) which relies on block-wise acquisition of *k*-space in subsequent echoes [99]; and (7) GRAPPATINI which is the combination of generalized autocalibrating partially parallel acquisition (GRAPPA)[100] and MARTINI [101]. 3D MUST-$T_2$ mapping has a high isotropic resolution yielding accurate results and can be acquired in only 8 minutes [98]. However, GRAPPATINI can acquire the whole-heart $T_2$ map in less than 4 minutes. These developments open the door to clinical feasibility. However, further studies are required to understand their accuracy and precision, before widespread clinical use.

Machine learning (ML) is a subcategory of Artificial intelligence (AI) which learns models from training data and applies them on new (i.e., testing) datasets with convolutional neural networks (CNNs) being a popular choice in radiology since they were designed to process imaging data [102]. In the context of CMR $T_2$ and $T_2$* mapping, the potential AI benefits on the horizon might include: (1) improving time efficiency of acquisition and reconstruction, (2) automated segmentation and calculation of metrics (structural or functional), and (3) development of new imaging biomarkers using texture analysis/radiomics (i.e., exploiting spatial heterogeneity of pixels) [103]. $T_2$ mapping acquisition can be accelerated without compromising on performance by combining a CNN with k-space undersampling as in Model-Augmented Neural network with Incoherent k-space Sampling (MANTIS) [104]. Similarly, CNNs, were employed for automated detection of cardiac landmarks yielding automated image delineation with a high accuracy whilst a manual assessment would have taken up to 20 minutes [105]. Pre-trained CNNs providing automated image segmentation for other tasks (e.g., $T_1$ mapping), can be adapted to automatically delineate $T_2$ maps through transfer learning bypassing the need to de novo retrain the network with $T_2$ mapping images [106]. Thus, transfer learning opens the door of standardization in fully automated cardiac mapping. Using stepwise dimension reduction and texture feature selection, texture analysis using $T_2$ mapping data might be able to capture subtle differences which could: (1) aid diagnostic challenges (e.g., diagnosing "dilated cardiomyopathy [DCM]-like" [107] or " myocardial infarction [MI]-like" acute myocarditis [108], and distinguishing cardiac amyloidosis from hypertrophic cardiomyopathy [HCM] [109]), (2) discriminate between myocardial areas of interest (e.g., distinguishing area at risk [AAR] from the infarct zone after an acute MI [110]), and (3) provide prognostic information (e.g., predicting major adverse cardiac events after an acute MI [111]). However, the widespread use of AI in $T_2$ and $T_2$* mapping, like with other CMR applications, is limited by: (1) lack of protocol standardization and transparency, (2) "black box" phenomena, (3) ethical considerations and (4) most studies are proof of concept retrospective studies which limit their generalization [103].

MR fingerprinting (MRF) refers to the acquisition of both $T_1$ and $T_2$ maps simultaneously. The natural co-registration of the maps can provide meaningful comparisons as $T_1$ and $T_2$ relaxation times can provide both additive and complementary information in different clinical settings [42]. For example, these co-registered maps might be better at characterizing myocardial diseases in which edema and fibrosis co-exist. By using pseudorandom pulse sequences in which the TR, TE, flip angle, and sample parameters are varied, MRF can generate spatial and temporal incoherence in which different tissues have different signal evolutions in time (i.e., fingerprints) due to their inherent $T_1$ and $T_2$ [112]. Examples include: (1) 3D-QALAS (3D-quanntification using an interleaved Look-Locker acquisition sequence with a $T_2$ preparation pulse) [113], (2) CABIRIA (cardiac balanced-SSFP inversion recovery with interleaved sampling acquisition), (3) multi-parametric Saturation-recovery single-Shot Acquisition (mSASHA) which is a modified version of SASHA for joint $T_1$–$T_2$ mapping in which saturation recovery and $T_2$ preparation is employed to acquire additional images [28], and (4) other joint $T_1$–$T_2$ mapping with $T_2$ preparation techniques [114], all capable of achieving accurate estimations of $T_1$ and $T_2$ times comparable to standard isolated $T_1$ and $T_2$ mapping. There is some evidence that these techniques may also help reduce the influence of $T_1$ and $T_2$ on the $T_2$ and $T_1$ maps respectively [115]. Future studies are required to improve the reliability of MFP and demonstrate their added clinical value.

## 5. Clinical applications

### 5.1. Myocardial infarction

CMR is the gold standard for quantifying the extent of a MI[116], but there is debate around which CMR sequence is best suited to do so. After a myocardial infarction the volume of damaged myocardium will increase from endocardium to epicardium in a transmural fashion (wavefront phenomenon theory) [117]. The myocardial AAR after an ischemic event consists of the non-viable necrotic zone and the salvageable peri-necrotic area. ischemic injury leads to cellular necrosis which activates a cytokine response that increases vascular permeability [118]. In addition, formerly intracellular contents (now interstitial) from necrotic cells exert an osmotic drag [119]. Thus, myocardial ischemia leads to edema through cytotoxic, osmotic, and vascular mechanisms, and consequently its $T_2$ time lengthens [120]. In addition,

acute MI is associated with gadolinium enhancement (GE) because cardiomyocyte death leaves more space for gadolinium to accumulate in the interstitial space compared to healthy myocardium. The endocardial to epicardial extent of infarction as assessed by late GE (LGE) was proposed to assess the AAR [121]. Compared to $T_2$-wegihted imaging, LGE underestimates AAR especially in those with early reperfusion [122,123]. Thus, $T_2$WI has been very useful clinically in distinguishing new infarcts from past ones. Historically, $T_2$WI was also used clinically to quantify the AAR in MI [124] as recommended by experts and society guidelines [125]. However, the AAR assessment is affected by the dynamic change of the extent of myocardial edema after ischemia and reperfusion and therefore, defining the time window for performing the CMR scan in the acute MI setting is important [126–129]. Thus, $T_2$WI imaging is not always reliable in quantifying the myocardial salvageable tissue [127,130]. By contrast, $T_2$ mapping distinguishes AAR from the infarct zone and healthy myocardium, despite not having prognostic value in predicting patient recovery [110]. However, it should be noted that this result was obtained using texture analyses rather than identifying $T_2$ value thresholds to distinguish AAR from the infarct zone. In non-ST elevation myocardial infarction (NSTEMI), $T_2$W STIR has lower diagnostic accuracy in detecting the infarct-related artery (as appraised by a combination of ECG and angiography) and underestimates the AAR compared to $T_2$ mapping [131]. Moreover, in reperfused STEMI, $T_2$ mapping is able to identify the necrotic region with a high accuracy (as appraised by LGE) and quantify the AAR [132]. The clinical superiority of $T_2$ mapping over $T_2$WI, relates to the fact that $T_2$ mapping is: (1) less susceptible to motion artifacts, (2) less prone to falsely elevate or mask $T_2$ values subendocardially, and (3) able to generate pixelwise quantitative $T_2$ maps making interpretation easier. However, $T_1$ mapping sees to perform just as well as $T_2$ mapping in quantifying the AAR in STEMI patients [133]. What is yet unclear is whether this comparable performance also holds true in NSTEMI patients.

Myocardial edema post-MI can affect both the systolic and diastolic function. Although controlling the myocardial edema through anti-inflammatory therapies post-MI is not standard practice currently on account of limited supportive evidence, this practice could change in the future [134]. Quantifying the extent and rate of myocardial edema resolution post-MI could become clinically relevant (Fig. 5) and $T_2$ mapping may be well equipped to do that, but no threshold to distinguish healthy myocardium from AAR [86] has yet been widely agreed yet. The main limitation rests with the need to have a full LV coverage in order to accurately estimate the AAR [135]. Although attempts, have been made to shorten the acquisition time to a 3-slice approach for clinically feasibility [136], this is less accurate when compared to full coverage mapping [135].

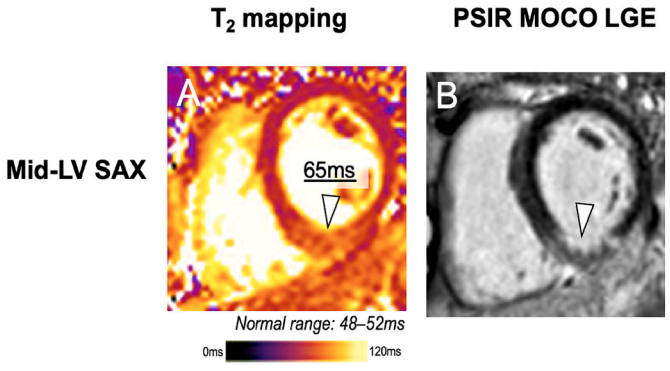


**Fig. 5.** $T_2$ mapping in acute MI. Mid LV SAX view showing features post-acute inferior MI (right coronary artery territory) with >50% wall thickness infarct-pattern LGE (subendocardial) in the mid inferior wall by PSIR MOCO LGE (**B**) and matching high $T_2$ (66 ms vs 49 ms in the remote anterior septum), (**A**). $T_2$ times are also abnormally long in the peri-infarct zone (at 56 ms).
*MI = myocardial infarction.* Other abbreviations as in Fig. 3.

In the context of MI, reduced oxygenated blood to the AAR increases the concentration of deoxygenated hemoglobin (Hb) [137]. Given its paramagnetic properties, the increased deoxygenated Hb is associated with decreased T2* times (known as the blood oxygenation level-dependent [BOLD] effect) [138] meaning that T2* can be regarded as a marker of myocardial oxygenations status [139,140]. In ischemia/reperfusion animal models, $T_2$* was shown to decrease in acute MI in the AAR, and then dynamically change during reperfusion suggesting that $T_2$* mapping might be able to distinguish acute from chronic MIs[141]. Moreover, $T_2$* mapping may additionally be employed to look for intramyocardial hemorrhage post-MI which associates with a worse prognosis[142,143].

### 5.2. *Myocardial infarction with non-obstructive coronary arteries (MINOCA)*

MINOCA encompasses a heterogeneous group of conditions leading to myocardial injury (scarring, i.e., focal fibrosis) in patients with angiographically non-obstructed coronary arteries [144]. The pathophysiological mechanisms of MINOCA are broadly divided into 4 categories [145]: (1) epicardial coronary abnormalities (spontaneous coronary dissection, epicardial artery spasm, coronary embolus/thrombus, coronary erosion/disruption); (2) microcirculatory abnormalities (coronary slow flow, microvascular angina, microvascular spasm); 3) myocardial causes (myocarditis, typical stress cardiomyopathy [aka Takotsubo], atypical stress cardiomyopathy, cardiomyopathy); 4) non-cardiac causes (hematological disorders, pulmonary embolism, renal dysfunction) [146]. When microcirculatory abnormalities lead to ischemia but fall short of causing detectable myocardial scarring, we term this ischemia with non-obstructive coronary arteries (INOCA)[147]. According to the European Society of Cardiology (ESC) working group position, MINOCA "should be considered as a 'working diagnosis' and thus prompts further evaluation regarding its underlying mechanism(s)" [148].

MINOCA is associated with morbidity and mortality [149] and given its broad etiology, $T_1$WI CMR is key to diagnosing its underlying cause as: (1) lLGE subendocardially suggests epicardial coronary MINOCA; (2) LGE subepicardially suggests myocardial MINOCA from myocarditis or cardiomyopathy; while (3) the absence of LGE typically favors stress cardiomyopathy. Still, a definitive diagnosis for MINOCA is not obtained despite CMR with LGE imaging in 10–20% of patients [148]. $T_2$ mapping can really help in such cases. For example, in typical stress cardiomyopathy (Fig. 6) $T_2$ mapping times are higher in myocardial areas displaying wall motion abnormalities compared to normokinetic regions [150], thus producing an almost pathognomonic base-to-apex gradient of ascending $T_2$ times mirroring the apical ballooning and hypokinesis. In addition, as discussed above, long $T_2$ times subendocardially would corroborate an acute atherosclerotic/non-atherosclerotic coronary MINOCA, while regional or widespread lengthening of myocardial $T_2$ times favor edema and therefore acute myocarditis (Fig. 7).

### 5.3. *Myocarditis*

As endomyocardial biopsy is invasive and prone to sampling errors, the Lake Louse Criteria (LLC) were proposed to assist with the diagnosis of acute myocarditis based on the presence of 2 of the following 3 CMR features: (1) edema on $T_2$WI, (2) hyperemia (with early GE [EGE]) and/or (3) necrosis or fibrosis (with LGE) [151]. However, the advent of myocardial $T_2$ mapping forced a redefinition of the LLC criteria in 2018 such that acute myocarditis can now be diagnosed if both $T_1$ (by $T_1$ mapping, extracellular volume [ECV], or LGE) and $T_2$ signals ($T_2$ mapping or hyperintensity on $T_2$ STIR) are increased [152]. The new LLC increased the sensitivity for acute myocarditis particularly if presentation was atypical [153].

Clinically, myocarditis is broadly divided into: (a) acute regional myocarditis [154], (b) acute panmyocarditis [155] and (c) chronic myocarditis [156]. Localized LGE suggests a regional myocarditis and

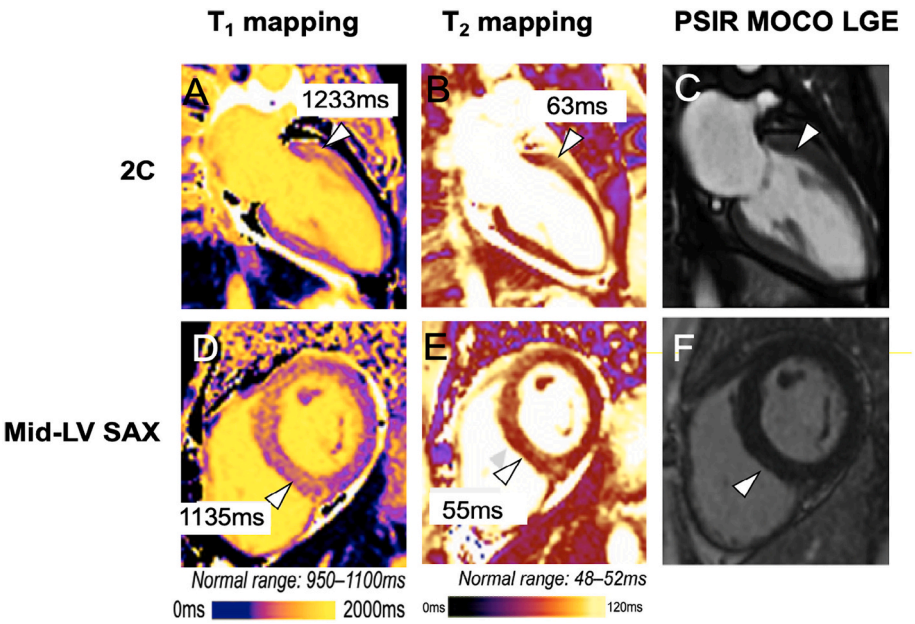


**Fig. 6.** $T_2$ mapping in a patient with atypical stress-induced cardiomyopathy developing after anesthesia induction in the context of thyrotoxicosis. 2C (top row, **A**–**C**) and mid LV SAX views (bottom row, **D**–**F**) showed no focal fibrosis by PSIR MOCO LGE but there was a zone of long $T_1$ and $T_2$ in the basal to mid anterior/septal wall. Abbreviations as in Fig. 3.

demonstrating long $T_2$ in the same region implies it is acute. In the rarer panmyocarditis, although there may not be any LGE, the diagnosis is clinched from the globally long $T_1$ and $T_2$ times. Although both $T_1$ and $T_2$ mapping can confirm or refute a diagnosis of acute myocarditis, only $T_2$ mapping can reliably diagnose chronic myocarditis (MyoRacer trial) [157], discriminate acute from healed myocarditis[158], and confirm myocarditis resolution over a 6 month follow up period [158]. An explanation for this could be that $T_1$ mapping cannot discern inflammatory from non-inflammatory cardiomyopathies especially where diffuse fibrosis co-exists as a confounder lengthening $T_1$ times in both scenarios [159]. Additionally, $T_2$ mapping can predict major adverse cardiac events and hospitalization following acute myocarditis [160].

Myocarditis received a lot of attention recently amidst the COVID-19 pandemic. Early studies reported that a degree of myocarditis is not uncommon among patients suffering from COVID-19 [161], especially if hospitalized [162]. However, COVID-19 myocarditis has been overemphasized as raised troponin in COVID-19 positive individuals is more likely to be related to macro- or micro-angiopathic thrombosis [163] than to actual myocarditis. Of course, true COVID-19 myocarditis does occur and although both $T_1$ and $T_2$ mapping are useful for its characterization, $T_2$ mapping might have a better diagnostic performance and correlation with high-sensitivity troponin T (hsTnT) levels, potentially reflecting the extent of acute myocardial edema [164,165]. The combination of $T_1$ and $T_2$ mapping could provide insights into the evolution of COVID-19 myocarditis: long $T_1$ and $T_2$ would suggest ongoing inflammation, while long $T_1$ and normal $T_2$ would suggest myocardial scarring [165]. However, the effects of COVID-19 on the heart and the role of mapping in COVID-19-related myocardial injury will be further elucidated once results from several large recent clinical trials become available (e.g., Cardiac Imaging in SARS-CoV-2 [CISCO-19] [166] with Clinical Trial identifier NCT04403607, COVID-HEART study with the International Standard Randomized Controlled Trial Number ISRCTN58667920). Myocarditis can also occur following COVID-19 mRNA vaccinations especially in males aged between 12 and 39 years (incidence 12.6 cases/1 million second dose of COVID-19 mRNA according to the US Center for Disease Control and Prevention [CDC][167]) [168]. Still, the benefits of vaccination outweigh such myocarditis risks, and COVID-19 vaccine primary series continues to be recommended for everyone aged 6 months or older as of July 2022 in the US [169].

Cardiac sarcoidosis is characterized by infiltrative sarcoid granulomas, and it is regarded as an inflammatory cardiomyopathy [170]. Long $T_2$ times occur in cardiac sarcoidosis [171,172] making $T_2$ mapping useful in identifying early cardiac involvement in systemic sarcoidosis [172].

Uremic myocarditis is a recognized complication in chronic kidney disease (CKD) especially when the glomerular filtration rate is less than 30 [173]. As native $T_1$ and $T_2$ mapping does not require intravenous contrast, they may be especially helpful to establish the diagnosis of uremic myocarditis.

### 5.4. *Infiltrative cardiomyopathies*

$T_2$ imaging is playing an increasingly important role in the infiltrative cardiomyopathies. Long $T_2$ times occur in amyloidosis and FD (where LVH is present [82], Fig. 8). In amyloidosis $T_2$ mapping correlates with histologically-proven edema [174] and it is able to partly distinguish light-chain (AL) from transthyretin amyloidosis (ATTR [175]), as well as treated from untreated AL [176]. In FD, long $T_2$ in the basal inferolateral (BIFL) wall, associates very strongly with troponin and N-terminal pro-brain natriuretic peptide (NT-proBNP) levels, ECG abnormalities, impaired longitudinal strain and worsening Fabry stabilization index [177]. Given the tight concordance between troponin and $T_2$ in BIFL, troponin has the potential to become an essential blood biomarker to follow up patients with FD being of course more cost-effective and readily available than CMR. Nonetheless, $T_2$ mapping remains an exciting FD biomarker as currently a patient's cardiac eligibility for enzyme replacement is mainly determined by the presence of LV hypertrophy which occurs later than $T_2$ changes and does not sensitively reflect the underlying pathological processes.

### 5.5. *Inherited cardiomyopathies*

CMR has become the gold-standard imaging modality for assessing non-ischemic cardiomyopathies [7]. In a recent meta-analysis, patients with DCM or HCM were shown to have longer $T_2$ times than healthy volunteers [82]. In addition, $T_2$ mapping can distinguish HCM from athlete's heart [178] and from other causes of pathological myocardial

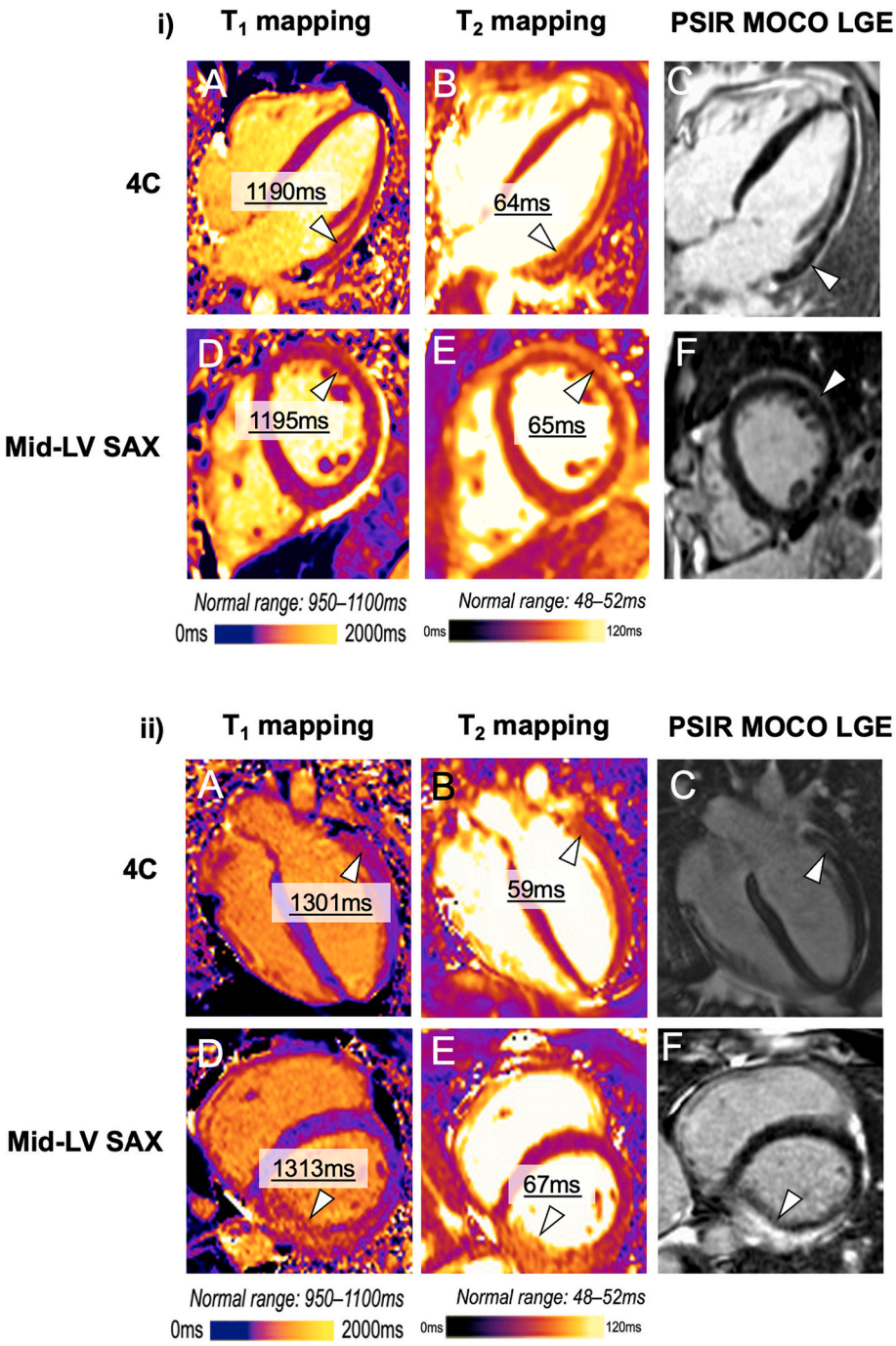


**Fig. 7.** $T_2$ mapping in two patients (i and ii) with acute myocarditis. 4C (top row, **A**–**C**) and mid LV SAX views (bottom, **D**–**F**). **i**) PSIR MOCO LGE showed subtle basal anterolateral midwall fibrosis with matching long $T_1$ and $T_2$ times. The long $T_2$ points to an acute process as long $T_1$ can be present in both fibrosis and edema. **ii**) Acute myocarditis affecting the basal inferior and inferolateral wall with high $T_1$, high $T_2$ and striking matching midwall to subepicardial LGE.
Abbreviations as in Fig. 3.

hypertrophy [179]. Moreover, certain non-hypertrophic normal contractile segments in HCM express longer $T_2$ times potentially highlighting areas with abnormal remodeling at tissue level prior to overt structural and functional changes [180]. Although $T_2$* values did not differ between patients with HCM and healthy controls [82], shorter $T_2$* times did associate with arrhythmic events in non-obstructive HCM [181].

### 5.6. Inflammatory phase of cardiomyopathies

Cardiomyopathies have been traditionally viewed as slow insidious processes progressively weakening the myocardium leading to failure. However, periods of disease exacerbations due to myocardial inflammation are increasingly recognized and referred to as the "inflammatory phase of cardiomyopathy". During such phases in patients with HCM, myocardial inflammation identified by CMR (Fig. 3) correlated with serological (e.g., high plasma cytokines and C-reactive protein [CRP]), histopathological (e.g., inflammatory cell infiltration on EMB) and immunological (e.g., increased nuclear factor kappa B [NF-kB] activation on immunohistochemistry) markers[182]. These inflammatory phases are thought to trigger myocardial fibrosis [183]. Since fibrosis is prevalent in cardiomyopathies [184], $T_1$ and ECV would be elevated regardless of the presence of edema. Thus, $T_2$ mapping is critical to distinguish active inflammation from this background fibrosis as not only is it sensitive to edema, but also immune to fibrosis-related confounding [86].

$T_2$ mapping can identify biopsy-confirmed myocardial inflammation in patients with DCM [185] while in HCM the presence of myocardial

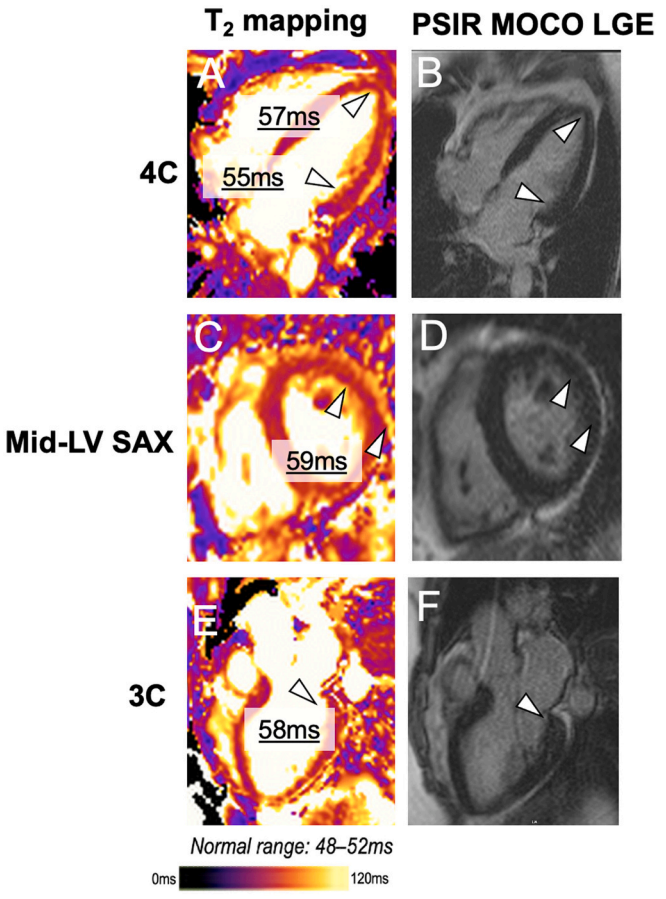


**Fig. 8.** $T_2$ mapping in a patient with Fabry disease and left ventricular hypertrophy. 4C (top row, **A**, **B**), mid LV SAX view (middle, **C**, **D**) and 2C view (bottom, **E**, **F**) showing mild concentric LV hypertrophy with loss of apical tapering. There is subtle patchy LGE in the apex and basal inferolateral wall with matching long $T_2$ (**A, C, E**). Abbreviations as in Fig. 3.

areas of long $T_2$ associate with increased hsTnT and BNP levels [186].

Whether longer $T_2$ times in the inflammatory phases of cardiomyopathy associate with adverse outcomes (e.g., faster disease progression, acute deterioration, arrhythmias, premature death etc.) is yet to be established.

### 5.7. Cardio-oncology

With the growing number of cancer patients and the advent of many novel cardiotoxic chemotherapy agents, cancer treatment-related cardiac dysfunction (CTRCD) has become a major cause of morbidity and mortality in this already vulnerable group of patients. Currently, performing serial echocardiograms is the gold standard for assessing cardiac function in cardio-oncology but tissue changes (e.g., edema, fibrosis etc.) appear long before functional changes reflected by changes in global longitudinal strain or ejection fraction (EF). This explains the increasingly important role of CMR in CTRCD [187]. While $T_1$ mapping can characterize early fibrosis, $T_2$ mapping can identify early edema which may be prognostically relevant. For example, regional myocardial edema as detected by $T_2$ mapping has been shown to predict cardiotoxicity in breast cancer patients whose regime involves sequential anthracyclines and trastuzumab [188].

Immune checkpoint proteins (e.g., cytotoxic T-lymphocyte associated protein 4 [CTLA-4], programmed cell death protein 1 [PD-1], programmed death ligand 1 [PDL-1] etc.) naturally occur on immune cells and their prime function is to dampen the immune response. When these proteins are expressed by cancer cells, they might avoid being killed by the T-cells. Thus, the advent of immune checkpoint inhibitors (ICI) meant increased overall survival and progression-free survival for patients suffering with various cancers (e.g., colon, lung etc.) [189]. However, the downside of ICI is uncontrolled inflammation in healthy tissues with the myocardium being a common site [190]. The result can be catastrophic as patients can rapidly progress from non-specifically symptomatic to full blown cardiogenic shock with premature mortality (up to 60% with nivolumab plus ipilimumab [191])[192]. As immunosuppressants (e.g., steroids) work well in autoimmune myocarditis [193], early recognition of ICI myocarditis can prompt the rapid initiation of treatment. $T_2$ mapping can be useful in detecting myocardial edema in ICI myocarditis [194] and to guide the initiation of treatment [195]. However, to date it was $T_1$ but not $T_2$ mapping which predicted major adverse cardiovascular events in a different study [196]. Data on the utility of $T_2$ mapping in ICI myocarditis is limited and larger scale studies are needed.

In addition, it has been postulated that $T_1$ and $T_2$ values might alter and re-normalize at different stages during chemotherapy suggesting that CTRCD may be a dynamic phenomenon, occurring in phases. This means that any mapping data should be interpreted within the chronological context of CMR relative to the stage of the chemotherapeutic regime [197]. The role of $T_1$ and $T_2$ mapping in chronic CTRCD is controversial and more research is required to inform decision-making.

### 5.8. Valve disease

Aortic stenosis (AS) is associated with cardiac remodeling and CMR mapping techniques play a role in characterizing this process. Patients with severe AS have higher $T_1$ and $T_2$ values suggesting a pathophysiological process involving inflammation and edema leading to diffuse myocardial fibrosis [198]. This is further supported by the fact that $T_2$ values decrease after transcatheter aortic valve replacement (TAVR) [199]. In addition, $T_2$ mapping might have a prognostic role in AS as LV lateral wall $T_2$ values correlate with the mean aortic valve gradient [200].

In addition to fibrosis, patients with degenerative valve prolapse (MVP) and mitral regurgitation (MR) might have subclinical myocardial edema [201] which could be explained by the inflammatory cell activation secondary to repetitive traction by leaflet movements [202]. As previously discussed, while $T_1$ mapping highlights the presence of fibrosis, $T_2$ mapping unmasks the edema making it well suited to detect inflammation. This might help identify individuals at risk of arrhythmias (as myocardial inflammation associates with electrical remodeling) and disease progression (as inflammation might translate into fibrosis) in the context of MVP/MR [203].

However, currently, there is no guideline-recommended role for $T_2$ imaging in valve disease.

### 5.9. Pulmonary arterial hypertension

CMR is the gold-standard for assessing RV volumes and function and it is recommended for the follow-up of patients with pulmonary arterial hypertension (PAH) by the ESC and European Respiratory Society (ERS) consensus guidelines [204]. Although $T_1$ mapping can detect early fibrosis, it does not provide prognostic information in the context of PAH [205]. To date, $T_2$ values have been observed to be higher in the RV insertion and RV free wall, and shown to correlate with RV end-diastolic volume index and RV mass index [200]. As end-systolic RV volume [206] and RV mass [207] are useful in the risk-stratification of patients with PAH, the prognostic value of $T_2$ mapping in PAH warrants further research. However, to date, the clinical value of $T_2$ imaging and mapping in PAH is yet to be established.

### 5.10. Heart transplant

Both DB $T_2$WI [208] and $T_2$ mapping [209] have a role in monitoring

the transplanted heart as longer $T_2$ times are observed on account of myocardial edema in acute rejection, which normalize following immunosuppressive treatment. $T_2$ mapping is preferable to biopsy as it is non-invasive and can characterize the entire myocardium reducing the risk of false-negatives due to inadequate sampling. Serial $T_2$ mapping post cardiac transplant could guide the up/down titration of immunosuppressive therapy [210]. This could supersede the current practice of monitoring therapeutic drug levels, as the immunotherapy would instead be tailored to the myocardial response to prevent rejection while minimizing the drug side effects. More work is needed to understand whether $T_2$ mapping could identify early-on those patients most at risk of developing transplant rejection. Currently, patients with graft rejection present rather late and most will therefore already have some degree of cardiovascular compromise that could cause irreversible myocardial damage shortening the lifespan of the graft. In addition to predicting transplant rejection, $T_2$ mapping of the transplanted heart has also been shown to predict adverse cardiac events (death, heart failure, myocardial infarction) [211,212].

### 5.11. Autoimmune rheumatological disorders

Many connective tissue diseases (CTDs) have a propensity to affect the heart leading to added morbidity and mortality. $T_1$, ECV and $T_2$ offer complementary information in the context of CTDs: $T_1$ mapping and ECV highlight inflammation, fibrosis and infiltration, while $T_2$ mapping highlights the edema [213]. As $T_1$ and ECV are both deranged in either fibrosis or inflammation which in fact often co-exist in CTDs, $T_1$ mapping is unreliable at identifying disease exacerbations or CTDs 'hot' phases. By contrast, $T_2$ mapping could point towards an acute process. However, its role in CTDs remains yet to be fully established in clinical practice as the inter-individual variability in $T_2$ relaxation times prevented the definition of cut-offs between physiological and pathological CTD states.

Lupus myocarditis is a rare, but a severe manifestation of systemic lupus erythematosus (SLE) which can lead to acute heart failure and even death. $T_2$ mapping can identify active myocardial involvement and correlate with the SLE disease activity index (SLEDAI) [214]. In addition, it can be used clinically to monitor the response to immunosuppressants as $T_2$ values shorten upon therapy initiation [215].

The main cause of death in systemic sclerosis (SS) is attributed to cardiac involvement [216]. Although a short burst of immunosuppressants can prevent the progression of myocardial damage and limit fibrosis, early detection of myocardial involvement is difficult as it can present with non-specific symptoms or be completely asymptomatic [217]. Although $T_1$ mapping and ECV are unreliable in detecting myocarditis in SS [218], $T_2$ mapping has been associated with ventricular arrhythmogenicity in SS 'hot' myocardial disease [219].

In addition, $T_2$ mapping is useful in diagnosing idiopathic inflammatory myopathy (IIM), but it is unable to distinguish IIM from viral myocarditis [220]. Conventional CMR like $T_1$WI and $T_2$WI can miss diffuse global edema, but a combination of long $T_2$ and $T_1$ and high ECV might help establish myocardial involvement even in atypical non-specific presentations of rare rheumatological conditions such as systemic capillary leak syndrome (SCLS) [221], ANCA (antineutrophil cytoplasmic antibody) associated vasculitidies (AAV) [222] or Anti-synthetase Syndrome [223].

### 5.12. Iron deposition

Myocardial iron deposition occurs in primary hemochromatosis, where there is uncontrolled iron absorption in the gut, and in transfusion-dependent patients (e.g., thalassemia major). Early identification and prompt treatment is vital as untreated iron overload can lead to DCM and heart failure. To control the circulating iron ions, the body chelates them with iron-binding proteins such as hemosiderin and ferritin, yet they still create distortions in the magnetic field causing the $T_2$* to decay faster than expected. Thus, $T_2$* mapping is the clinical imaging biomarker of choice to assess myocardial iron (Fig. 9). $T_2$* mapping can predict echocardiographically confirmed left ventricular impairment secondary to iron overload [224]. $T_2$* of <20ms (mild to moderate iron overload) is also prognostically useful having been associated with an increased risk of arrythmia, while $T_2$* <10ms (severe iron overload) is strongly associated with heart failure [52]. $T_2$* mapping can be used to guide the timing of chelation therapy and to monitor its effectiveness [225].

### 5.13. The role of $T_1$ mapping in identifying myocardial edema

While $T_2$ mapping is more commonly used to identify myocardial edema and has been the focus of this review, it is important to clarify that there is also a role for $T_1$ mapping [126] in this space. For example, the shortened version of MOLLI (shMOLLI) [226] has a higher heart rate and $T_1$ independence over a wider range of $T_1$ values and might have a better diagnostic performance in identifying edema compared to $T_2$WI in Takotsubo cardiomyopathy or acute regional myocardial edema without infarction [92]. In reperfused STEMI, MOLLI $T_1$ mapping had a similar performance as $T_2$ prepared bSSFP $T_2$ mapping in delimiting the AAR and quantifying the infarct size [133]. Therefore, $T_1$ mapping has the potential to complement $T_2$ mapping in identifying myocardial edema which warrants its further investigation in research settings [126]. However, it should be noted that $T_1$ is lengthened in both edema and fibrosis, while longer $T_2$ times are most obvious in edema [86].

## 6. Conclusion

$T_2$ mapping in CMR has almost completely replaced conventional $T_2$WI as the sequence of choice to highlight myocardial edema, and therefore inflammation if linked to troponin. It has the potential to improve the diagnostic accuracy in MINOCA, delineate salvageable myocardium after an MI, monitor for cardiotoxicity in cancer patients, and serve as a surrogate end point in clinical trials for anti-inflammatory therapies in myocarditis or in the inflammatory phase of an inherited cardiomyopathy.

$T_2$* mapping which assesses myocardial iron, has the potential to guide the timing of chelation therapy and monitor its effectiveness [225]. It could be further developed to predict the development of LV failure and arrythmias in patients with hemochromatosis.

$T_2$ mapping and $T_2$* mapping are key diagnostic and prognostic biomarkers in clinical CMR. Innovative approaches promise faster acquisitions and tantalizingly also whole-heart coverage, but innovation will need to go hand in hand with sequence standardization and quality assurance, to ensure the widest and best possible use of $T_2$ and $T_2$* imaging to guide clinical care.

## 7. Equations

Equation 1:

$$\frac{1}{T_2^*} = \frac{1}{T_{2\ true}} + \frac{1}{T_{2\ inhomogeneities}}, where\ \frac{1}{T_{2\ inhomogeneities}} = \gamma \Delta B_0$$

$T_2$* – measured transverse relaxation time

$T_{2\ true}$ – true tissue transverse relaxation in the absence of any tissue inhomogeneities

$T_{2\ inhomogeneities}$ – transverse relaxation due to magnetic field inhomogeneities

$\gamma$ – gyromagnetic ratio

$\Delta B_0$ – differences in magnetic field inhomogeneities across a voxel

## Compliance with ethical standards

All procedures performed were in accordance with the ethical standards of the institutional and/or national research committee and with

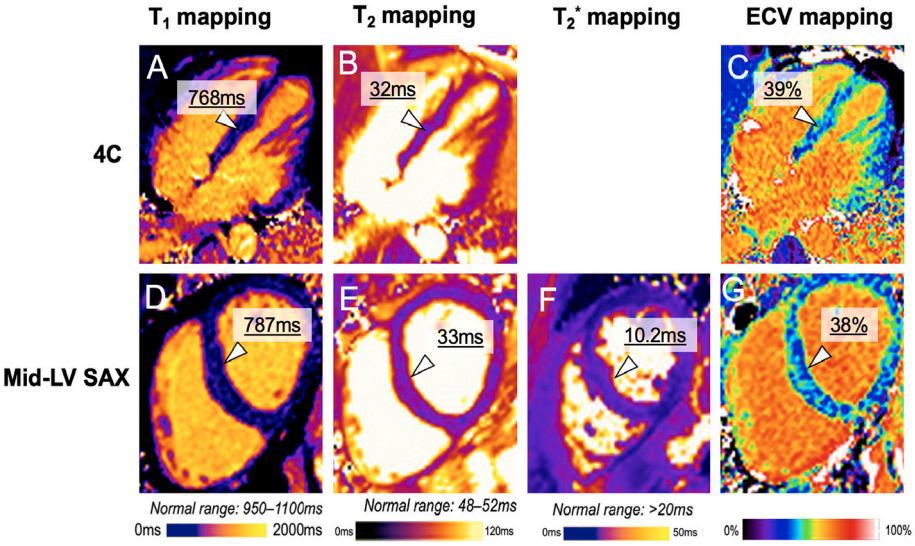


**Fig. 9.** $T_2$* mapping in a patient with liver transplant and previous alcohol excess now showing iron overload cardiomyopathy. 4C (top row, **A–C**) and mid LV SAX views (bottom, **D–G**). $T_2$* mapping shows major myocardial iron overload accompanied by short $T_1$, high ECV and short $T_2$. Please note that the $T_1$ mapping was acquired pre-contrast.

the 1964 Helsinki declaration and its later amendments or comparable ethical standards. As the data used in this manuscript is publicly available, an ethics approval waiver was applied.

## Sources of funding

.

G.C. is supported by the British Heart Foundation (BHF, SP/20/2/34841), the BHF Accelerator Award (AA/18/6/34223) and by the National Institute of Health Research (NIHR) UCL Hospitals Biomedical Research Centre (BRC). G.C. and J.C.M. a are supported by the Barts Charity HeartOME1000 Grant (MGU0427/G-001411). J.C.M. is directly and indirectly supported by the UCL Hospitals NIHR BRC and Biomedical Research Unit at Barts Hospital respectively.

## Role of the funding source

None of the funders was involved in the study design, the collection, the analysis, the interpretation of the data, and in the decision to submit the article for publication.

## Author contributions

All authors contributed significantly to the design, implementation, analysis, interpretation, and manuscript writing. The corresponding author attests that all listed authors meet the authorship criteria and that no others meeting the criteria have been omitted.

## Data availability

All the relevant data has been published in the manuscript.

## Permissions

Clinical images (Figs. 3 and 5–9) were acquired by the authors, while the schematic diagrams (Figs. 1, 2, and 4) were created by the authors. Therefore, no requests for permissions to reproduce figures were made.

ECV = extracellular volume. Other abbreviations as in Fig. 3.

## Declaration of Competing Interest

The views expressed in this article are those of the authors who declare that they have no conflict of interest.

## References

[1] Frangogiannis NG. The inflammatory response in myocardial injury, repair, and remodelling. Nat Rev Cardiol 2014;11(5):255–65.
[2] Kiamanesh O, Toma M. The state of the heart biopsy: a clinical review. CJC Open (Online) 2021;3(4):524–31.
[3] Jacob R, Khan M. Cardiac biomarkers: what is and what can be. Indian J Cardiovasc Dis Women 2018;3(4):240–4.
[4] Li J, Cao T, Wei Y, Zhang N, Zhou Z, Wang Z, et al. A review of novel cardiac biomarkers in acute or chronic cardiovascular diseases: the role of soluble ST2 (sST2), lipoprotein-associated phospholipase A2 (Lp-PLA2), myeloperoxidase (MPO), and procalcitonin (PCT). Dis Markers 2021;2021. 6258865-10.
[5] Ding Y, Wang Y, Zhang W, Jia Q, Wang X, Li Y, et al. Roles of biomarkers in myocardial fibrosis. Aging Dis 2020;11(5):1157–74.
[6] Richards AM. Future biomarkers in cardiology: my favourites. Eur Heart J Suppl 2018;20(suppl_G):G37–44.
[7] Captur G, Manisty C, Moon JC. Cardiac MRI Evaluation of Myocardial Disease. 2016.
[8] Radenkovic D, Weingärtner S, Ricketts L, Moon JC, Captur G. T1 mapping in cardiac MRI. Heart Fail Rev 2017;22(4):415–30.
[9] Kramer CM, Barkhausen J, Bucciarelli-Ducci C, Flamm SD, Kim RJ, Nagel E. Standardized cardiovascular magnetic resonance imaging (CMR) protocols: 2020 update. J Cardiovasc Magn Reson 2020;22(1). 17-.
[10] Bloch F. Nuclear induction. Physica 1951;17(3):272–81.
[11] Nitz WR, Reimer P. Contrast mechanisms in MR imaging. Eur Radiol 1999;9(6):1032–46.
[12] Currie S, Hoggard N, Craven IJ, Hadjivassiliou M, Wilkinson ID. Understanding MRI: basic MR physics for physicians. Postgrad Med J 2013;89(1050):209–23.
[13] Chavhan GB, Babyn PS, Thomas B, Shroff MM, Mark Haacke E. Principles, techniques, and applications of T2-based MR imaging and its special applications. Radiographics 2009;29(5):1433–49.
[14] Dabir D, Child N, Kalra A, Rogers T, Gebker R, Jabbour A, et al. Reference values for healthy human myocardium using a T1 mapping methodology: results from the International T1 Multicenter cardiovascular magnetic resonance study. J Cardiovasc Magn Reson 2014;16(1). 69-.
[15] Bojorquez JZ, Bricq S, Acquitter C, Brunotte F, Walker PM, Lalande A. What are normal relaxation times of tissues at 3 T? Magn Reson Imaging 2017;35:69–80.
[16] Hanson CA, Kamath A, Gottbrecht M, Ibrahim S, Salerno M. T2 relaxation times at cardiac MRI in healthy adults: a systematic review and meta-analysis. Radiology 2020;297(2):344–51.
[17] Elster AD. An index system for comparative parameter weighting in MR imaging. J Comput Assist Tomogr 1988;12(1):130–4.
[18] Ridgway JP. Cardiovascular magnetic resonance physics for clinicians: Part i. J Cardiovasc Magn Reson 2010;12(1). 71-.
[19] Hahn EL. Spin echoes. Phys Rev 1950;80(4):580–94.
[20] Elster AD. Gradient-echo MR imaging: techniques and acronyms. Radiology 1993;186(1):1–8.

[21] Bloembergen N, Purcell EM, Pound RV. Relaxation effects in nuclear magnetic resonance absorption. Phys Rev 1948;73(7):679–712.
[22] Whittall KP, MacKay AL, Graeb DA, Nugent RA, Li DKB, Paty DW. In vivo measurement of T-2 distributions and water contents in normal human brain. Magn Reson Med 1997;37(1):34–43.
[23] Biglands JD, Radjenovic A, Ridgway JP. Cardiovascular magnetic resonance physics for clinicians: Part II. J Cardiovasc Magn Reson 2012;14(1). 66-.
[24] Edelman RR, Chien D, Kim D. Fast selective black blood MR imaging. Radiology 1991;181(3):655–60.
[25] Bydder GM, Young IR. MR imaging: Clinical use of the inversion recovery sequence. J Comput Assist Tomogr 1985;9(4):659–75.
[26] Liu Y, Riederer SJ, Ehman RL. Magnetization-prepared cardiac imaging using gradient echo acquisition. Magn Reson Med 1993;30(2):271–5.
[27] Patel MR, Klufas RA, Alberico RA, Edelman RR. Half-fourier acquisition single-shot turbo spin-echo (HASTE) MR: comparison with fast spin-echo MR in diseases of the brain. Am J Neuroradiol AJNR 1997;18(9):1635–40.
[28] Kellman P, Xue H, Chow K, Howard J, Chacko L, Cole G, et al. Bright-blood and dark-blood phase sensitive inversion recovery late gadolinium enhancement and T1 and T2 maps in a single free-breathing scan: an all-in-one approach. J Cardiovasc Magn Reson 2021;23:2021. Article 126.
[29] Krinsky G, Rofsky NM, Weinreb JC. Nonspecificity of short inversion time inversion recovery (STIR) as a technique of fat suppression: pitfalls in image interpretation. Am J Roentgenol 1996;166(3):523–6.
[30] Hargreaves B. Rapid gradient-echo imaging. J Magn Reson Imaging 2012;36(6):1300–13.
[31] Scheffler K, Lehnhardt S. Principles and applications of balanced SSFP techniques. Eur Radiol 2003;13(11):2409–18.
[32] Kellman P, Aletras AH, Mancini C, McVeigh ER, Arai AE. T2-prepared SSFP improves diagnostic confidence in edema imaging in acute myocardial infarction compared to turbo spin echo. Magn Reson Med 2007;57(5):891–7.
[33] Chavhan GB, Babyn PS, Jankharia BG, Cheng H-LM, Shroff MM. Steady-state MR imaging sequences: physics, classification, and clinical applications. Radiographics 2008;28(4):1147–60.
[34] Ferreira PF, Gatehouse PD, Mohiaddin RH, Firmin DN. Cardiovascular magnetic resonance artefacts. J Cardiovasc Magn Reson 2013;15(1). 41-.
[35] Levitt MH, Freeman R. Compensation for pulse imperfections in NMR spin-echo experiments. J Magn Reson 1969;43(1):65–80. 1981.
[36] Brittain JH, Hu BS, Wright GA, Meyer CH, Macovski A, Nishimura DG. Coronary angiography with magnetization-prepared T2 contrast. Magn Reson Med 1995;33(5):689–96.
[37] Shea SM, Deshpande VS, Chung Y-C, Li D. Three-dimensional true-FISP imaging of the coronary arteries: Improved contrast with T2-preparation. J Magn Reson Imaging 2002;15(5):597–602.
[38] Levitt M, Freeman R, Frenkiel T. Supercycles for broadband hetero-nuclear decoupling. J Magn Reson 1982;50:157–60.
[39] Salerno M, Kramer CM. Advances in parametric mapping with cardiac magnetic resonance imaging. J Am Coll Cardiol Img 2013;6(7):806–22.
[40] Lota AS, Gatehouse PD, Mohiaddin RH. T2 mapping and T2 imaging in heart failure. Heart Fail Rev 2017;22(4):431–40.
[41] Giri S, Chung Y-C, Merchant A, Mihai G, Rajagopalan S, Raman SV, et al. T2 quantification for improved detection of myocardial edema. J Cardiovasc Magn Reson 2009;11(1). 56-.
[42] Messroghli DR, Moon JC, Ferreira VM, Grosse-Wortmann L, He T, Kellman P, et al. Clinical recommendations for cardiovascular magnetic resonance mapping of T1, T2, T2* and extracellular volume: a consensus statement by the Society for Cardiovascular Magnetic Resonance (SCMR) endorsed by the European Association for Cardiovascular Imaging (EACVI). J Cardiovasc Magn Reson 2017;19:2017. Article 75.
[43] He T, Gatehouse PD, Anderson LJ, Tanner M, Keegan J, Pennell DJ, et al. Development of a novel optimized breathhold technique for myocardial T2 measurement in thalassemia. J Magn Reson Imaging 2006;24(3):580–5.
[44] Kim D, Jensen JH, Wu EX, Sheth SS, Brittenham GM. Breathhold multiecho fast spin-echo pulse sequence for accurate R2 measurement in the heart and liver. Magn Reson Med 2009;62(2):300–6.
[45] Baeßler B, Schaarschmidt F, Stehning C, Schnackenburg B, Maintz D, Bunck AC. A systematic evaluation of three different cardiac T2-mapping sequences at 1.5 and 3T in healthy volunteers. Eur J Radiol 2015;84(11):2161–70.
[46] Oshio K, Feinberg DA. GRASE (gradient-and spin-echo) imaging: a novel fast MRI technique. Magn Reson Med 1991;20(2):344–9.
[47] Basha T, Akcakaya M, Roujol S, Nezafat R. Precision and reproducibility of T2 quantifications in myocardial T2 mapping: impact of the number of echoes and reconstruction model. J Cardiovasc Magn Reson 2015;17(S1). W9-W.
[48] Zur Y, Wood ML, Neuringer LJ. Spoiling of transverse magnetization in steady-state sequences. Magn Reson Med 1991;21(2):251–63.
[49] Foltz WD, Al-Kwifi O, Sussman MS, Stainsby JA, Wright GA. Optimized spiral imaging for measurement of myocardial T2 relaxation. Magn Reson Med 2003;49(6):1089–97.
[50] Huang T-Y, Liu Y-J, Stemmer A, Poncelet BP. T2 measurement of the human myocardium using a T2-prepared transient-state trueFISP sequence. Magn Reson Med 2007;57(5):960–6.
[51] Wang C, Jang J, Neisius U, Nezafat M, Fahmy A, Kang J, et al. Black blood myocardial T2 mapping. Magn Reson Med 2019;81(1):153–66.
[52] Triadyaksa P, Oudkerk M, Sijens PE. Cardiac T2 mapping: techniques and clinical applications. J Magn Reson Imaging 2020;52(5):1340–51.
[53] Kellman P, Xue H, Spottiswoode BS, Sandino CM, Hansen MS, Abdel-Gadir A, et al. Free-breathing T2 mapping using respiratory motion corrected averaging. J Cardiovasc Magn Reson 2015;17(1). 3-.
[54] Carpenter J-P, He T, Kirk P, Roughton M, Anderson LJ, De Noronha SV, et al. On T2 magnetic resonance and cardiac iron. Circulation (New York, NY) 2011;123(14):1519–28.
[55] He T, Gatehouse PD, Kirk P, Tanner MA, Smith GC, Keegan J, et al. Black-blood T2 technique for myocardial iron measurement in thalassemia. J Magn Reson Imaging 2007;25(6):1205–9.
[56] Menacho K, Abdel-Gadir A, Moon JC, Fernandes JL. T2*mapping techniques iron overload assessment and other potential clinical applications. Magn Reson Imaging Clin N Am 2019;27(3):439–51.
[57] Westwood M, Anderson LJ, Firmin DN, Gatehouse PD, Charrier CC, Wonke B, et al. A single breath-hold multiecho T2 cardiovascular magnetic resonance technique for diagnosis of myocardial iron overload. J Magn Reson Imaging 2003;18(1):33–9.
[58] Ghugre NR, Enriquez CM, Coates TD, Nelson Jr MD, Wood JC. Improved R2 measurements in myocardial iron overload. J Magn Reson Imaging 2006;23(1):9–16.
[59] Saiviroonporn P, Viprakasit V, Boonyasirinant T, Khuhapinant A, Wood JC, Krittayaphong R. Comparison of the region-based and pixel-wise methods for cardiac T2 analysis in 50 transfusion-dependent Thai thalassemia patients. J Comput Assist Tomogr 2011;35(3):375–81.
[60] Wantanajittikul K, Theera-Umpon N, Saekho S, Auephanwiriyakul S, Phrommintikul A, Leemasawat K. Automatic cardiac T2 relaxation time estimation from magnetic resonance images using region growing method with automatically initialized seed points. Comput Methods Prog Biomed 2016;130:76–86.
[61] Zheng Q, Feng Y, Wei X, Feng M, Chen W, Lu Z, et al. Automated interventricular septum segmentation for black-blood myocardial T2 measurement in thalassemia. J Magn Reson Imaging 2015;41(5):1242–50.
[62] He T, Zhang J, Carpenter J-P, Feng Y, Smith GC, Pennell DJ, et al. Automated truncation method for myocardial T2 measurement in thalassemia. J Magn Reson Imaging 2013;37(2):479–83.
[63] Sandino CM, Kellman P, Arai AE, Hansen MS, Xue H. Myocardial T2 mapping: influence of noise on accuracy and precision. J Cardiovasc Magn Reson 2015;17(1). 7-.
[64] Jin N, Da Silveira JS, Jolly M-P, Firmin DN, Mathew G, Lamba N, et al. Free-breathing myocardial T2 mapping using GRE-EPI and automatic Non-rigid motion correction. J Cardiovasc Magn Reson 2015;17(1). 113-.
[65] Schweser F, Deistung A, Lehr BW, Reichenbach JR. Differentiation between diamagnetic and paramagnetic cerebral lesions based on magnetic susceptibility mapping. Med Phys (Lancaster) 2010;37(10):5165–78.
[66] Yu H, McKenzie CA, Shimakawa A, Vu AT, Brau ACS, Beatty PJ, et al. Multiecho reconstruction for simultaneous water-fat decomposition and T2 estimation. J Magn Reson Imaging 2007;26(4):1153–61.
[67] Ma J. Dixon techniques for water and fat imaging. J Magn Reson Imaging 2008;28(3):543–58.
[68] Dixon WT. Simple proton spectroscopic imaging. Radiology 1984;153(1):189–94.
[69] Moon JC, Messroghli DR, Kellman P, Piechnik SK, Robson MD, Ugander M, et al. Myocardial T1 mapping and extracellular volume quantification: a Society for Cardiovascular Magnetic Resonance (SCMR) and CMR Working Group of the European Society of Cardiology consensus statement. J Cardiovasc Magn Reson 2013;15(1). 92-.
[70] Messroghli DR, Radjenovic A, Kozerke S, Higgins DM, Sivananthan MU, Ridgway JP. Modified Look-Locker inversion recovery (MOLLI) for high-resolution T1 mapping of the heart. Magn Reson Med 2004;52(1):141–6.
[71] Chow K, Flewitt JA, Green JD, Pagano JJ, Friedrich MG, Thompson RB. Saturation recovery single-shot acquisition (SASHA) for myocardial T 1 mapping. Magn Reson Med 2014;71(6):2082–95.
[72] Weingärtner S, Akçakaya M, Basha T, Kissinger KV, Goddu B, Berg S, et al. Combined saturation/inversion recovery sequences for improved evaluation of scar and diffuse fibrosis in patients with arrhythmia or heart rate variability: improved Imaging of scar/fibrosis. Magn Reson Med 2014;71(3):1024–34.
[73] Higgins DM, Ridgway JP, Radjenovic A, Sivananthan UM, Smith MA. T1 measurement using a short acquisition period for quantitative cardiac applications: T1 measurement for cardiac applications. Med Phys (Lancaster) 2005;32(6Part1):1738–46.
[74] Robson MD, Piechnik SK, Tunnicliffe EM, Neubauer S. T1 measurements in the human myocardium: the effects of magnetization transfer on the SASHA and MOLLI sequences. Magn Reson Med 2013;70(3):664–70.
[75] Kellman P, Hansen MS. T1-mapping in the heart: accuracy and precision. J Cardiovasc Magn Reson 2014;16(1). 2-.
[76] Kellman P, Herzka DA, Arai AE, Hansen MS. Influence of off-resonance in myocardial T1-mapping using SSFP based MOLLI method. J Cardiovasc Magn Reson 2013;15(1). 63-.
[77] Kawel N, Nacif M, Zavodni A, Jones J, Liu S, Sibley CT, et al. T1 mapping of the myocardium: intra-individual assessment of post-contrast T1 time evolution and extracellular volume fraction at 3T for Gd-DTPA and Gd-BOPTA. J Cardiovasc Magn Reson 2012;14(1). 26-.
[78] Roy C, Slimani A, De Meester C, Amzulescu M, Pasquet A, Vancraeynest D, et al. Age and sex corrected normal reference values of T1, T2 T2*and ECV in healthy subjects at 3T CMR. J Cardiovasc Magn Reson 2017;19(1). 72-.
[79] Granitz M, Motloch LJ, Granitz C, Meissnitzer M, Hitzl W, Hergan K, et al. Comparison of native myocardial T1 and T2 mapping at 1.5T and 3T in healthy

volunteers: reference values and clinical implications. Wien Klin Wochenschr 2018;131(7–8):143–55.
[80] Wiesmueller M, Wuest W, Heiss R, Treutlein C, Uder M, May MS. Cardiac T2 mapping: robustness and homogeneity of standardized in-line analysis. J Cardiovasc Magn Reson 2020;22(1). 39-.
[81] Von Knobelsdorff-Brenkenhoff F, Prothmann M, Dieringer MA, Wassmuth R, Greiser A, Schwenke C, et al. Myocardial T1 and T2 mapping at 3 T: reference values, influencing factors and implications. J Cardiovasc Magn Reson 2013;15 (1). 53-.
[82] Snel GJH, van den Boomen M, Hernandez LM, Nguyen CT, Sosnovik DE, Velthuis BK, et al. Cardiovascular magnetic resonance native T2 and T2 quantitative values for cardiomyopathies and heart transplantations: a systematic review and meta-analysis. J Cardiovasc Magn Reson 2020;22(1). 34-.
[83] Poller L. International normalized ratios (INR): the first 20 years. J Thromb Haemost 2004;2(6):849–60.
[84] Captur G, Bhandari A, Brühl R, Ittermann B, Keenan KE, Yang Y, et al. T1 mapping performance and measurement repeatability: results from the multi-national T1 mapping standardization phantom program (T1MES). J Cardiovasc Magn Reson 2020;22(1). Article 31.
[85] Seo HS, Captur G, Ittermann B, Pang W, Keenan K, Kellman P, et al. 27A medical device grade T2 phantom to quality control inflammation imaging by CMR. Eur Heart J Cardiovasc Imaging 2019;20(Supplement_2).
[86] Montant P, Sigovan M, Revel D, Douek P. MR imaging assessment of myocardial edema with T2 mapping. Diagn Interv Imaging 2015;96(9):885–90.
[87] Thavendiranathan P, Walls M, Giri S, Verhaert D, Rajagopalan S, Moore S, et al. Improved detection of myocardial involvement in acute inflammatory cardiomyopathies using T2 mapping. Circ Cardiovasc Imaging 2012;5(1):102–10.
[88] Yang H-J, Sharif B, Pang J, Kali A, Bi X, Cokic I, et al. Fast, free-breathing, whole-heart cardiac magnetic resonance T2 mapping for myocardial edema imaging. Circulation (New York, NY) 2014;130(22).
[89] Ding H, Fernandez-de-Manuel L, Schär M, Schuleri KH, Halperin H, He L, et al. Three-dimensional whole-heart T2 mapping at 3T. Magn Reson Med 2015;74(3): 803–16.
[90] Basha TA, Bellm S, Roujol S, Kato S, Nezafat R. Free-breathing slice-interleaved myocardial T2 mapping with slice-selective T2 magnetization preparation. Magn Reson Med 2016;76(2):555–65.
[91] Jeserich M, Kimmel S, Maisch P, von Rauffer S, Achenbach S. The best way to assess oedema using T1, T2 mapping or three-dimensional T2-weighted fast-spin-echo triple inversion recovery sequences via cardiovascular MRI in outpatients with suspected myocarditis. Clin Radiol 2020;75(5):383–9.
[92] Ferreira VM, Piechnik SK, Dallarmellina E, Karamitsos TD, Francis JM, Choudhury RP, et al. Non-contrast T1-mapping detects acute myocardial edema with high diagnostic accuracy: a comparison to T2-weighted cardiovascular magnetic resonance. J Cardiovasc Magn R 2012;14(1). 42-.
[93] Cocker MS, Shea SM, Strohm O, Green J, Abdel-Aty H, Friedrich MG. A New approach towards improved visualization of myocardial edema using T2-weighted imaging: a cardiovascular magnetic resonance (CMR) study. J Magn Reson Imaging 2011;34(2):286–92.
[94] Graff C, Li Z, Bilgin A, Altbach M, Gmitro A, Clarkson E. <h1 data-selenium-selector="paper-detail-title"> Iterative T2 estimation from highly undersampled radial fast spin-echo data. Proc Intl Soc Mag Reson Med 2006;14:925.
[95] Block KT, Uecker M, Frahm J. Model-based iterative reconstruction for radial fast spin-echo MRI. TMI 2009;28(11):1759–69.
[96] Lugand E, Yerly J, Feliciano H, Chaptinel J, Stuber M, van Heeswijk RB. Accelerated and KWIC-filtered cardiac T2 mapping for improved precision: proof of principle. J Cardiovasc Magn Reson 2015;17(S1). W30-W.
[97] Lugand E, Yerly J, Feliciano H, Chaptinel J, Stuber M, van Heeswijk RB. Breath-held high-resolution cardiac T2 mapping with SKRATCH. J Cardiovasc Magn Reson 2016;18(422).
[98] Bustin A, Milotta G, Ismail TF, Neji R, Botnar RM, Prieto C. Accelerated free-breathing whole-heart 3D T2 mapping with high isotropic resolution. Magn Reson Med 2020;83(3):988–1002.
[99] Sumpf TJ, Uecker M, Boretius S, Frahm J. Model-based nonlinear inverse reconstruction for T2 mapping using highly undersampled spin-echo MRI. J Magn Reson Imaging 2011;34(2):420–8.
[100] Griswold MA, Jakob PM, Heidemann RM, Nittka M, Jellus V, Wang J, et al. Generalized autocalibrating partially parallel acquisitions (GRAPPA). Magn Reson Med 2002;47(6):1202–10.
[101] Wang F, Zhang H, Wu C, Wang Q, Hou B, Sun Y, et al. Quantitative T2 mapping accelerated by GRAPPATINI for evaluation of muscles in patients with myositis. Brit J Radiol 2019;92(1102). 20190109-.
[102] Yamashita R, Nishio M, Do RKG, Togashi K. Convolutional neural networks: an overview and application in radiology. Insights Imaging 2018;9(4):611–29.
[103] Fotaki A, Puyol-Antón E, Chiribiri A, Botnar R, Pushparajah K, Prieto C. Artificial intelligence in cardiac MRI: is clinical adoption forthcoming? Front Cardiovasc Med 2021;8. 818765-.
[104] Liu F, Feng L, Kijowski R. MANTIS: Model-Augmented Neural neTwork with Incoherent k-Space Sampling for Efficient MR T2 Mapping. 2018.
[105] Xue H, Artico J, Fontana M, Moon JC, Davies RH, Kellman P. Landmark detection in cardiac MRI by using a convolutional neural network. Radiol Artif Intell 2021;3 (5). e200197-e.
[106] Zhu Y, Fahmy AS, Duan C, Nakamori S, Nezafat R. Automated myocardial T2 and extracellular volume quantification in cardiac MRI using transfer learning-based myocardium segmentation. Radiol Artif Intell 2020;2(1). e190034-e.
[107] Baessler B, Luecke C, Klingel K, Kandolf R, Schuler G, Maintz D, et al. P2583Texture analysis and machine learning applied on cardiac magnetic resonance T2 mapping: incremental diagnostic value in biopsy-proven acute myocarditis. Eur Heart J 2017;38(suppl_1).
[108] Baessler B, Luecke C, Lurz J, Klingel K, Von Roeder M, De Waha S, et al. Cardiac MRI texture analysis of T1 and T2 maps in patients with infarctlike acute myocarditis. Radiology 2018;289(2):357–65.
[109] Huang S, Shi K, Zhang Y, Yan W-F, Guo Y-K, Li Y, et al. Texture analysis of T2-weighted cardiovascular magnetic resonance imaging to discriminate between cardiac amyloidosis and hypertrophic cardiomyopathy. BMC Cardiovasc Disord 2022;22(1). 235-.
[110] Fan Zi-Yang, Wu Chong-Wen, An Dong-Aolei, Chen Bing-Hua, Wesemann Luke D, He Jie, Hu Jia-Ni, Bu Jun, Xu Jian-Rong, Zhou Yan, Wu Lian-Ming. Myocardial area at risk and salvage in reperfused acute MI measured by texture analysis of cardiac T2 mapping and its prediction value of functional recovery in the convalescent stage. Int J Card Imaging 2021;37(12):3549–60. https://doi.org/10.1007/s10554-021-02336-7. Epub 2021 Jul 19.
[111] Fan ZY, Wu CW, Wesemann LD, Ouchi E, Bautista M, Qiu J, et al. Predictive value of major adverse cardiac events by T2-mapping texture analysis of the myocardial remote zone in patients with acute myocardial infarction. Clin Radiol 2022;77(3). e241-e9.
[112] Ma D, Gulani V, Seiberlich N, Liu K, Sunshine JL, Duerk JL, et al. Magnetic resonance fingerprinting. Nature 2013;495(7440):187–92.
[113] Kvernby S, MJAB Warntjes, Haraldsson H, Carlhäll C-J, Engvall J, Ebbers T. Simultaneous three-dimensional myocardial T1 and T2 mapping in one breath hold with 3D-QALAS. J Cardiovasc Magn R 2014;16(1). 102-.
[114] Akçakaya M, Weingärtner S, Basha TA, Roujol S, Bellm S, Nezafat R. Joint myocardial T1 and T2 mapping using a combination of saturation recovery and T2-preparation. Magn Reson Med 2016;76(3):888–96.
[115] Chow K, Hayes G, Flewitt JA, Feuchter P, Lydell C, Howarth A, et al. Improved Accuracy and Precision In Simultaneous Myocardial T1 and T2 Mapping with Multi-Parametric SASHA (mSASHA). 2021.
[116] Thiele H, Kappl MJE, Conradi S, Niebauer J, Hambrecht R, Schuler G. Reproducibility of chronic and acute infarct size measurement by delayed enhancement-magnetic resonance imaging. J Am Coll Cardiol 2006;47(8): 1641–5.
[117] Reimer KA, Lowe JE, Rasmussen MM, Jennings RB. The wavefront phenomenon of ischemic cell death. 1. Myocardial infarct size vs duration of coronary occlusion in dogs. Circulation (New York, NY) 1977;56(5):786–94.
[118] Neumann F-J, Ott I, Gawaz M, Richardt G, Holzapfel H, Jochum M, et al. Cardiac release of cytokines and inflammatory responses in acute myocardial infarction. Circulation (New York, NY) 1995;92(4):748–55.
[119] Galluzzi L, Vitale I, Aaronson SA, Abrams JM, Adam D, Agostinis P, et al. Molecular Mechanisms of Cell Death: Recommendations of the Nomenclature Committee on Cell Death 2018. 2018.
[120] Carrick D, Haig C, Ahmed N, Rauhalammi S, Clerfond G, Carberry J, et al. Temporal evolution of myocardial hemorrhage and edema in patients after acute ST-segment elevation myocardial infarction: pathophysiological insights and clinical implications. J Am Heart Assoc 2016;5(2). n/a.
[121] Kim RJ, Fieno DS, Parrish TB, Harris K, Chen E-L, Simonetti O, et al. Relationship of MRI delayed contrast enhancement to irreversible injury, infarct age, and contractile function. Circulation (New York, NY) 1999;100(19):1992–2002.
[122] Ubachs J, Engblom H, Erlinge D, Jovinge S, Hedström E, Carlsson M, et al. Cardiovascular magnetic resonance of the myocardium at risk in acute reperfused myocardial infarction: comparison of T2-weighted imaging versus the circumferential endocardial extent of late gadolinium enhancement with transmural projection. J Cardiovasc Magn Reson 2010;12(1). 18-.
[123] Friedrich MGMD, Abdel-Aty HMD, Taylor AMD, Schulz-Menger JMD, Messroghli DMD, Dietz RMD. The salvaged area at risk in reperfused acute myocardial infarction as visualized by cardiovascular magnetic resonance. J Am Coll Cardiol 2008;51(16):1581–7.
[124] Wright J, Adriaenssens T, Dymarkowski S, Desmet W, Bogaert J. Quantification of myocardial area at risk with T2-weighted CMR. Comparison with contrast-enhanced CMR and coronary angiography. JACC-Cardiovasc Imaging 2009;2(7): 825–31.
[125] Stillman AE, Oudkerk M, Bluemke D, Bremerich J, Esteves FP, Garcia EV, et al. Assessment of acute myocardial infarction: current status and recommendations from the North American society for cardiovascular imaging and the European society of cardiac radiology. Int J Card Imaging 2011;27(1):7–24.
[126] Bulluck H, Dharmakumar R, Arai AE, Berry C, Hausenloy DJ. Cardiovascular Magnetic Resonance in Acute ST-Segment-Elevation Myocardial Infarction: Recent Advances, Controversies, and Future Directions. 2018.
[127] Carrick D, Haig C, Ahmed N, Rauhalammi S, Clerfond G, Carberry J, et al. Temporal evolution of myocardial hemorrhage and edema in patients after acute ST-segment elevation myocardial infarction: pathophysiological insights and clinical implications. J Am Heart Assoc 2016;5(2). n/a.
[128] Fernández-Jiménez R, Sánchez-González J, Agüero J, García-Prieto J, López-Martín GJ, García-Ruiz JM, et al. Myocardial edema after ischemia/reperfusion is not stable and follows a bimodal pattern: Imaging and histological tissue characterization. J Am Coll Cardiol 2015;65(4):315–23.
[129] Bulluck H, Hammond-Haley M, Weinmann S, Martinez-Macias R, Hausenloy DJ. Myocardial infarct size by CMR in clinical cardioprotection studies insights from randomized controlled. Trials 2017;10(3):230–40. https://doi.org/10.1016/j.jcmg.2017.01.008.
[130] Kim HW, Van Assche L, Jennings RB, Wince WB, Jensen CJ, Rehwald WG, et al. Relationship of T2-weighted MRI myocardial hyperintensity and the ischemic area-at-risk. Circ Res 2015;117(3):254–65.

[131] Layland J, Rauhalammi S, Lee MMY, Ahmed N, Carberry J, Teng Yue May V, et al. Diagnostic accuracy of 3.0-T magnetic resonance T1 and T2 mapping and T2-weighted dark-blood imaging for the infarct-related coronary artery in non-ST-segment elevation myocardial infarction. J Am Heart Assoc 2017;6(4).
[132] Bulluck H, White SK, Rosmini S, Bhuva A, Treibel TA, Fontana M, et al. T1 mapping and T2 mapping at 3T for quantifying the area-at-risk in reperfused STEMI patients. J Cardiovasc Magn Reson 2015;17(1). 73-.
[133] Bulluck H, Hammond-Haley M, Fontana M, Knight DS, Sirker A, Herrey AS, et al. Quantification of both the area-at-risk and acute myocardial infarct size in ST-segment elevation myocardial infarction using T1-mapping. J Cardiovasc Magn Reson 2017;19:2017. Article 57.
[134] Huang S, Frangogiannis NG. Anti-inflammatory therapies in myocardial infarction: failures, hopes and challenges. Br J Pharmacol 2018;175(9):1377–400.
[135] Bulluck H, Bryant JA, Lim MX, Tan XW, Ramlall M, Francis R, et al. Full Left Ventricular Coverage is Essential for the Accurate Quantification of the Area- at-Risk by T1 and T2 Mapping. 2017.
[136] Hamshere S, Jones DA, Pellaton C, Longchamp D, Burchell T, Mohiddin S, et al. Cardiovascular magnetic resonance imaging of myocardial oedema following acute myocardial infarction: Is whole heart coverage necessary? J Cardiovasc Magn Reson 2016;18(1). 7-.
[137] Bauer WR, Nadler W, Bock M, Schad LR, Wacker C, Hartlep A, et al. The relationship between the BOLD-induced T2 and T2/: a theoretical approach for the vasculature of myocardium. Magn Reson Med 1999;42(6):1004–10.
[138] Guensch DP, Michel MC, Huettenmoser SP, Jung B, Gulac P, Segiser A, et al. The blood oxygen level dependent (BOLD) effect of in-vitro myoglobin and hemoglobin. Sci Rep 2021;11(1). 11464-.
[139] Manka R, Paetsch I, Schnackenburg B, Gebker R, Fleck E, Jahnke C. BOLD cardiovascular magnetic resonance at 3.0 tesla in myocardial ischemia. J Cardiovasc Magn Reson 2010;12(1). 54-.
[140] Wacker CM, Hartlep AW, Pfleger S, Schad LR, Ertl G, Bauer WR. Susceptibility-sensitive magnetic resonance imaging detects human myocardium supplied by a stenotic coronary artery without a contrast agent. J Am Coll Cardiol 2003;41(5):834–40.
[141] Aguor ENE, Arslan F, vDCWA Kolk, MGJ Nederhoff, PAFM Doevendans, vCJA Echteld, et al. Quantitative T2 assessment of acute and chronic myocardial ischemia/reperfusion injury in mice. Magma (New York, NY) 2012;25(5):369–79.
[142] Zia MI, Ghugre NR, Connelly KA, Strauss BH, Sparkes JD, Dick AJ, et al. Characterizing myocardial edema and hemorrhage using quantitative T2 and T2 mapping at multiple time intervals post ST-segment elevation myocardial infarction. Circ Cardiovasc Imaging 2012;5(5):566–72.
[143] Robbers LFHJ, Nijveldt R, Beek AM, Teunissen PFA, Hollander MR, Biesbroek PS, et al. The influence of microvascular injury on native T1 and T2 relaxation values after acute myocardial infarction: implications for non-contrast-enhanced infarct assessment. Eur Radiol 2018;28(2):824–32.
[144] Scalone G, Niccoli G, Crea F. Editor's choice- pathophysiology, diagnosis and management of MINOCA: an update. Eur Heart J Acute Cardiovasc Care 2019;8(1):54–62.
[145] Pelliccia F, Marzilli M, Boden WE, Camici PG. Why the term MINOCA does not provide conceptual clarity for actionable decision-making in patients with myocardial infarction with no obstructive coronary artery disease. J Clin Med 2021;10(20):4630.
[146] Singh T, Chapman AR, Dweck MR, Mills NL, Newby DE. MINOCA: a heterogenous group of conditions associated with myocardial damage. Heart 2021;107(18):1458–64. https://doi.org/10.1136/heartjnl-2020-318269. heartjnl-2020-318269.
[147] Pacheco Claudio C, Quesada O, Pepine CJ, Merz Noel Bairey, C.. Why names matter for women: MINOCA/INOCA (myocardial infarction/ischemia and no obstructive coronary artery disease). Clin Cardiol (Mahwah, NJ) 2018;41(2):185–93.
[148] Agewall S, Beltrame JF, Reynolds HR, Niessner A, Rosano G, Caforio ALP, et al. ESC working group position paper on myocardial infarction with non-obstructive coronary arteries. Eur Heart J 2017;38(3):143–53.
[149] Eggers KM, Hjort M, Baron T, Jernberg T, Nordenskjöld AM, Tornvall P, et al. Morbidity and cause-specific mortality in first-time myocardial infarction with nonobstructive coronary arteries. J Intern Med 2019;285(4):419–28.
[150] Vermes E, Pericart L, Pucheux J, Delhommais A, Alison D, Genee O. T2-mapping and T1-mapping detect myocardial involvement inTako-Tsubo cardiomyopathy: a preliminary experience. J Cardiovasc Magn Reson 2015;17(S1). 1-.
[151] Friedrich MGMD, Sechtem UMD, Schulz-Menger JMD, Holmvang GMD, Alakija PMD, Cooper LTMD, et al. Cardiovascular magnetic resonance in myocarditis: a JACC white paper. J Am Coll Cardiol 2009;53(17):1475–87.
[152] Ferreira VM, Schulz-Menger J, Holmvang G, Kramer CM, Carbone I, Sechtem U, et al. Cardiovascular magnetic resonance in nonischemic myocardial inflammation: expert recommendations. J Am Coll Cardiol 2018;72(24):3158–76.
[153] Cundari G, Galea N, De Rubeis G, Frustaci A, Cilia F, Mancuso G, et al. Use of the new Lake Louise criteria improves CMR detection of atypical forms of acute myocarditis. Int J Cardiovasc Imaging 2021;37(4):1395–404.
[154] Miklozek CL, Crumpacker CS, Royal HD, Come PC, Sullivan JL, Abelmann WH. Myocarditis presenting as acute myocardial infarction. Am Heart J 1988;115(4):768–76.
[155] Frustaci A, Scarpa M, Maria da Riol R, Agrati C, Finato N, Verardo R, et al. Fabry cardiomyopathy: Gb3-induced auto-reactive panmyocarditis requiring heart transplantation. ESC Heart Fail 2020;7(3):1331–7.
[156] Sagar SMD, Liu PPP, Cooper LTP. Myocarditis. Lancet (British Edition) 2012;379(9817):738–47.
[157] Lurz P, Luecke C, Eitel I, Föhrenbach F, Frank C, Grothoff M, et al. Comprehensive cardiac magnetic resonance imaging in patients with suspected myocarditis: the MyoRacer-trial. J Am Coll Cardiol 2016;67(15):1800–11.
[158] von Knobelsdorff-Brenkenhoff F, Schüler J, Dogangüzel S, Dieringer MA, Rudolph A, Greiser A, et al. Detection and monitoring of acute myocarditis applying quantitative cardiovascular magnetic resonance. Circ Cardiovasc Imaging 2017;10(2).
[159] Pan JA, Lee YJ, Salerno M. Diagnostic performance of extracellular volume, native T1, and T2 mapping versus Lake Louise criteria by cardiac magnetic resonance for detection of acute myocarditis: a meta-analysis. Circ Cardiovasc Imaging 2018;11(7). e007598-e.
[160] Spieker M, Haberkorn S, Gastl M, Behm P, Katsianos S, Horn P, et al. Abnormal T2 mapping cardiovascular magnetic resonance correlates with adverse clinical outcome in patients with suspected acute myocarditis. J Cardiovasc Magn Reson 2017;19(1). 38-.
[161] Catapano F, Marchitelli L, Cundari G, Cilia F, Mancuso G, Pambianchi G, et al. Role of advanced imaging in COVID-19 cardiovascular complications. Insights Imaging 2021;12(1). 28-.
[162] Knight DS, Kotecha T, Razvi Y, Chacko L, Brown JT, Jeetley PS, et al. COVID-19: myocardial injury in survivors. Circulation 2020;2020.
[163] Imazio M, Klingel K, Kindermann I, Brucato A, De Rosa FG, Adler Y, et al. COVID-19 pandemic and troponin: indirect myocardial injury, myocardial inflammation or myocarditis? Heart 2020;106(15):1127–31.
[164] Galea N, Marchitelli L, Pambianchi G, Catapano F, Cundari G, Birtolo LI, et al. T2-mapping increase is the prevalent imaging biomarker of myocardial involvement in active COVID-19: a Cardiovascular Magnetic Resonance study. J Cardiovasc Magn Reson 2021;23(1). 68-.
[165] Puntmann VO, Carerj ML, Wieters I, Fahim M, Arendt C, Hoffmann J, et al. Outcomes of cardiovascular magnetic resonance imaging in patients recently recovered from coronavirus disease 2019 (COVID-19). JAMA Cardiol 2020;5(11):1265–73.
[166] Mangion K, Morrow A, Bagot C, Bayes H, Blyth KG, Church C, et al. The chief scientist office cardiovascular and pulmonary imaging in SARS coronavirus disease-19 (CISCO-19) study. Cardiovasc Res 2020;116(14):2185–96.
[167] Gargano JW, Wallace M, Hadler SC, Langley G, Su JR, Oster ME, et al. Use of mRNA COVID-19 vaccine after reports of myocarditis among vaccine recipients: update from the advisory committee on immunization practices - United States, June 2021. MMWR Morb Mortal Wkly Rep 2021;70(27):977–82.
[168] Bozkurt B, Kamat I, Hotez PJ. Myocarditis with COVID-19 mRNA Vaccines. Circulation (New York, NY) 2021;144(6):471–84.
[169] CDC. Stay Up to Date with Your COVID-19 Vaccines. Centers for Disease Control and Prevention; 2022. https://www.cdc.gov/coronavirus/2019-ncov/vaccines/stay-up-to-date.html;.
[170] Doughan AR, Williams BR. Cardiac sarcoidosis. Heart 2006;92(2):282–8.
[171] Crouser ED, Ono C, Tran T, He X, Raman SV. Improved detection of cardiac sarcoidosis using magnetic resonance with myocardial T2 mapping. Am J Respir Crit Care Med 2014;189(1):109–12.
[172] Puntmann VO, Isted A, Hinojar R, Foote L, Carr-White G, Nagel E. T1 and T2 mapping in recognition of early cardiac involvement in systemic sarcoidosis. Radiology 2017;285(1):63–72.
[173] Garikapati K, Goh D, Khanna S, Echampati K. Uraemic cardiomyopathy: a review of current literature. Clin Med Insights Cardiol 2021;15. 1179546821998347-.
[174] Banypersad SM. The evolving role of cardiovascular magnetic resonance imaging in the evaluation of systemic amyloidosis. Magn Reson Insights 2019;12. 1178623X19843519-1178623X.
[175] Ridouani F, Damy T, Tacher V, Derbel H, Legou F, Sifaoui I, et al. Myocardial native T2 measurement to differentiate light-chain and transthyretin cardiac amyloidosis and assess prognosis. J Cardiovasc Magn Reson 2018;20(1). 58-.
[176] Kotecha T, Martinez-Naharro A, Treibel TA, Francis R, Nordin S, Abdel-Gadir A, et al. Myocardial edema and prognosis in amyloidosis. J Am Coll Cardiol 2018;71(25):2919–31.
[177] Augusto JB, Nordin S, Vijapurapu R, Baig S, Bulluck H, Castelletti S, et al. Myocardial Edema, myocyte injury, and disease severity in fabry disease. Circ Cardiovasc Imaging 2020;13(3). Article e010171.
[178] Gastl M, Lachmann V, Christidi A, Janzarik N, Veulemans V, Haberkorn S, et al. Cardiac magnetic resonance T2 mapping and feature tracking in athlete's heart and HCM. Eur Radiol 2021;31(5):2768–77.
[179] Arcari L, Hinojar R, Engel J, Freiwald T, Platschek S, Zainal H, et al. Native T1 and T2 provide distinctive signatures in hypertrophic cardiac conditions – comparison of uremic, hypertensive and hypertrophic cardiomyopathy. Int J Cardiol 2020;306:102–8.
[180] Huang L, Ran L, Zhao P, Tang D, Han R, Ai T, et al. MRI native T1 and T2 mapping of myocardial segments in hypertrophic cardiomyopathy: Tissue remodeling manifested prior to structure changes. Brit J Radiol 2019;92(1104). 20190634-.
[181] Gastl M, Gruner C, Labucay K, Gotschy A, Von Spiczak J, Polacin M, et al. Cardiovascular magnetic resonance T2 mapping for the assessment of cardiovascular events in hypertrophic cardiomyopathy. Open Heart 2020;7(1). e001152-e.
[182] Kuusisto J, Kärjä V, Sipola P, Kholová I, Peuhkurinen K, Jääskeläinen P, et al. Low-grade inflammation and the phenotypic expression of myocardial fibrosis in hypertrophic cardiomyopathy. Heart 2012;98(13):1007–13.
[183] Westermann D. Does inflammation trigger fibrosis in hypertrophic cardiomyopathy: a burning question? Heart 2012;98(13):965–6.
[184] Hinderer S, Schenke-Layland K. Cardiac fibrosis – a short review of causes and therapeutic strategies. Adv Drug Deliv Rev 2019;146:77–82.

[185] Spieker M, Katsianos E, Gastl M, Behm P, Horn P, Jacoby C, et al. T2 mapping cardiovascular magnetic resonance identifies the presence of myocardial inflammation in patients with dilated cardiomyopathy as compared to endomyocardial biopsy. Eur Heart J Cardiovasc Img 2018;19(5):574–82.
[186] Amano Y, Yanagisawa F, Tachi M, Hashimoto H, Imai S, Kumita S. Myocardial T2 mapping in patients with hypertrophic cardiomyopathy. J Comput Assist Tomogr 2017;41(3):344–8.
[187] de Baat EC, Naaktgeboren WR, Leiner T, Teske AJ, Habets J, Grotenhuis HB. Update in imaging of cancer therapy-related cardiac toxicity in adults. Open Heart 2021;8(1).
[188] Thavendiranathan P, Amir E, Bedard P, Crean A, Paul N, Nguyen ET, et al. Regional myocardial edema detected by T2 mapping is a feature of cardiotoxicity in breast cancer patients receiving sequential therapy with anthracyclines and trastuzumab. J Cardiovasc Magn Reson 2014;16(S1). P273-P.
[189] Robert C. A decade of immune-checkpoint inhibitors in cancer therapy. Nat Commun 2020;11(1). 3801-.
[190] Leuschner F, Katus HA, Kaya Z. Autoimmune myocarditis: past, present and future. J Autoimmun 2009;33(3):282–9.
[191] Johnson DB, Balko JM, Compton ML, Chalkias S, Gorham J, Xu Y, et al. Fulminant myocarditis with combination immune checkpoint blockade. New Engl J Med 2016;375(18):1749–55.
[192] Tajiri K, Aonuma K, Sekine I. Immune checkpoint inhibitor-related myocarditis. Jpn J Clin Oncol 2018;48(1):7–12.
[193] Bruestle K, Hackner K, Kreye G, Heidecker B. Autoimmunity in acute myocarditis: how immunopathogenesis steers new directions for diagnosis and treatment. Curr Cardiol Rep 2020;22(5). 28-.
[194] Semper H, Muehlberg F, Schulz-Menger J, Allewelt M, Grohé C. Drug-induced myocarditis after nivolumab treatment in a patient with PDL1- negative squamous cell carcinoma of the lung. Lung Cancer 2016;99:117–9.
[195] Ida M, Nakamori S, Ishida M, Dohi K. Management of immune checkpoint inhibitor myocarditis: a serial cardiovascular magnetic resonance T2 mapping approach. Eur Heart J 2021;42(29). 2869-.
[196] Thavendiranathan P, Zhang L, Zafar A, Drobni ZD, Mahmood SS, Cabral M, et al. Myocardial T1 and T2 mapping by magnetic resonance in patients with immune checkpoint inhibitor–associated myocarditis. J Am Coll Cardiol 2021;77(12):1503–16.
[197] Löffler AI, Salerno M. Cardiac MRI for the evaluation of oncologic cardiotoxicity. J Nucl Cardiol 2018;25(6):2148–58.
[198] Fehrmann A, Treutlein M, Rudolph T, Rudolph V, Weiss K, Giese D, et al. Myocardial T1 and T2 mapping in severe aortic stenosis: potential novel insights into the pathophysiology of myocardial remodelling. Eur J Radiol 2018;107:76–83.
[199] Gastl M, Behm P, Haberkorn S, Holzbach L, Veulemans V, Jacoby C, et al. Role of T2 mapping in left ventricular reverse remodeling after TAVR. Int J Cardiol 2018;266:262–8.
[200] Wang J, Zhao H, Wang Y, Herrmann HC, Witschey WRT, Han Y. Native T1 and T2 mapping by cardiovascular magnetic resonance imaging in pressure overloaded left and right heart diseases. J Thorac Dis 2018;10(5):2968–75.
[201] Miller MA, Adams DH, Pandis D, Robson PM, Pawale A, Pyzik R, et al. Hybrid positron emission tomography/magnetic resonance imaging in arrhythmic mitral valve prolapse. JAMA Cardiol 2020;5(9):1000–6.
[202] Kitkungvan D, Nabi F, Kim RJ, Bonow RO, Khan MA, Xu J, et al. Myocardial fibrosis in patients with primary mitral regurgitation with and without prolapse. J Am Coll Cardiol 2018;72(8):823–34.
[203] Pradella S, Grazzini G, Miele V. Mitral valve prolapse imaging: the role of tissue characterization. Quant Imaging Med Surg 2020;10(12):2396–400.
[204] Galie N, Torbicki A, Barst R, Dartevelle P, Haworth S, Higenbottam T, et al. Guidelines on diagnosis and treatment of pulmonary arterial hypertension: The Task Force on Diagnosis and Treatment of Pulmonary Arterial Hypertension of the European Society of Cardiology. Eur Heart J 2004;25(24):2243–78.
[205] Saunders LC, Johns CS, Stewart NJ, Oram CJE, Capener DA, Puntmann VO, et al. Diagnostic and prognostic significance of cardiovascular magnetic resonance native myocardial T1 mapping in patients with pulmonary hypertension. J Cardiovasc Magn R 2018;20(1). 78-.
[206] Lewis RA, Johns CS, Cogliano M, Capener D, Tubman E, Elliot CA, et al. Identification of cardiac magnetic resonance imaging thresholds for risk stratification in pulmonary arterial hypertension. Am J Respir Crit Care Med 2020;201(4):458–66.
[207] Simpson CE, Damico RL, Kolb TM, Mathai SC, Khair RM, Sato T, et al. Ventricular mass as a prognostic imaging biomarker in incident pulmonary arterial hypertension. Eur Respir J 2019;53(4):1802067.
[208] Marie PY, Angioï M, Bertrand A, Walker PM, Villemot JP, Carteaux JP, et al. Detection and prediction of acute heart transplant rejection with the myocardial T2 determination provided by a black-blood magnetic resonance imaging sequence. J Am Coll Cardiol 2001;37(3):825–31.
[209] Usman AA, Taimen K, Markl M, Carr JC, Wasielewski M, McDonald J, et al. Cardiac magnetic resonance T2 mapping in the monitoring and follow-up of acute cardiac transplant rejection: a pilot study. Circ Cardiovasc Imaging 2012;5(6):782–90.
[210] Butler CR, Savu AM, Bakal JA, Toma M, Thompson R, Chow K, et al. Correlation of cardiovascular magnetic resonance imaging findings and endomyocardial biopsy results in patients undergoing screening for heart transplant rejection. J Heart Lung Transplant 2015;34(5):643–50. https://doi.org/10.1016/j.healun.2014.12.020.
[211] Chaikriangkrai K, Abbasi MA, Sarnari R, Dolan R, Lee D, Anderson AS, et al. Prognostic value of myocardial extracellular volume fraction and T2-mapping in heart transplant patients. J Am Coll Cardiol Img 2020;13(7):1521–30.
[212] Abbasi M, Sarnari R, Chaikriangkrai K, Jivan A, Blaisdell J, Ghafourian K, et al. Myocardial T2-mapping predicts adverse cardiac events in heart transplantation patients. J Am Coll Cardiol 2020;75(11). 1573-.
[213] Baeßler B, Emrich T. The role of cardiovascular magnetic resonance imaging in rheumatic heart disease. Clin Exp Rheumatol 2018;36(5):S171–6.
[214] Ardoin S, Jarjour W, Raman S, Kibler A, Tran T. CMR with Quantitative T2 Mapping in Patients with Active SLE. ACR/ARHP Annual Meeting Abstracts: American College of Rheumatology. 2014.
[215] Hinojar R, Foote L, Sangle S, Marber M, Mayr M, Carr-White G, et al. Native T1 and T2 mapping by CMR in lupus myocarditis: disease recognition and response to treatment. Int J Cardiol 2016;222:717–26.
[216] Steen VD, Medsger TA. Changes in causes of death in systemic sclerosis, 1972–2002. Ann Rheum Dis 2007;66(7):940–4.
[217] Pieroni MMDP, De Santis MMDP, Zizzo GMDP, Bosello SMDP, Smaldone CMD, Campioni MP, et al. Recognizing and treating myocarditis in recent-onset systemic sclerosis heart disease: potential utility of immunosuppressive therapy in cardiac damage progression. Semin Arthritis Rheum 2014;43(4):526–35.
[218] Markousis-Mavrogenis G, Koutsogeorgopoulou L, Katsifis G, Dimitroulas T, Kolovou G, Kitas GD, et al. The double-edged sword of t1-mapping in systemic sclerosis-a comparison with infectious myocarditis using cardiovascular magnetic resonance. Diagnostics (Basel) 2020;10(5):335.
[219] Mavrogeni S, Gargani L, Pepe A, Monti L, Markousis-Mavrogenis G, Koutsogeorgopoulou L, et al. The relationship between arrhythmogenicity and novel parametric cardiac magnetic resonance indices in systemic sclerosis patients. 41. Eur Heart J 2020;59(8):1938–48. https://doi.org/10.1093/rheumatology/kez494.
[220] Huber AT, Bravetti M, Lamy J, Bacoyannis T, Roux C, De Cesare A, et al. Non-invasive differentiation of idiopathic inflammatory myopathy with cardiac involvement from acute viral myocarditis using cardiovascular magnetic resonance imaging T1 and T2 mapping. J Cardiovasc Magn R 2018;20(1). 11-.
[221] Urmeneta Ulloa J, Martínez de Vega V, Salvador Montañés O, Álvarez Vázquez A, Sánchez-Enrique C, Hernández Jiménez S, et al. Cardiac magnetic resonance in recovering COVID-19 patients. Feature tracking and mapping analysis to detect persistent myocardial involvement. Int J Cardiol Heart Vasculature 2021;36.100854-.
[222] Greulich S, Mayr A, Kitterer D, Latus J, Henes J, Steubing H, et al. T1 and T2 mapping for evaluation of myocardial involvement in patients with ANCA-associated vasculitides. J Cardiovasc Magn R 2017;19(1). 6-.
[223] Sado DM, Kozor R, Corr L, Moon JC. Global myocardial edema in antisynthetase syndrome detected by cardiovascular magnetic resonance mapping techniques. Circulation 2016;133(3):e25–6.
[224] Meloni A, Restaino G, Borsellino Z, Caruso V, Spasiano A, Zuccarelli A, et al. Different patterns of myocardial iron distribution by whole-heart T2 magnetic resonance as risk markers for heart complications in thalassemia major. Int J Cardiol 2014;177(3):1012–9.
[225] Chen X, Zhang Z, Zhong J, Yang Q, Yu T, Cheng Z, et al. MRI assessment of excess cardiac iron in thalassemia major: when to initiate? J Magn Reson Imaging 2015;42(3):737–45.
[226] Piechnik SK, Ferreira VM, Dall'Armellina E, Cochlin LE, Greiser A, Neubauer S, et al. Shortened Modified Look-Locker Inversion recovery (ShMOLLI) for clinical myocardial T1-mapping at 1.5 and 3 T within a 9 heartbeat breathhold. J Cardiovasc Magn Reson 2010;12(1). 69-.
[227] Hennig J, Nauerth A, Friedburg H. RARE imaging: a fast imaging method for clinical MR. Magn Reson Med 1986;3(6):823–33.
[228] Simonetti OP, Finn JP, White RD, Laub G, Henry DA. "Black blood" T2-weighted inversion-recovery MR imaging of the heart. Radiology 1996;199(1):49–57.
[229] Haase A, Frahm J, Matthaei D, Hanicke W, Merboldt KD. FLASH imaging. Rapid NMR imaging using low flip-angle pulses. J Magn Reson 1969;67(2):258–66. 1986.
[230] Scheffler K, Hennig J. Is TrueFISP a gradient-echo or a spin-echo sequence? Magn Reson Med 2003;49(2):395–7.
[231] Baeßler B, Schaarschmidt F, Stehning C, Schnackenburg B, Maintz D, Bunck AC. Cardiac T2-mapping using a fast gradient echo spin echo sequence - first in vitro and in vivo experience. J Cardiovasc Magn Reson 2015;17(1). 67-.
[232] Feinberg DA, Kiefer B, Johnson G. GRASE improves spatial resolution in single shot imaging. Magn Reson Med 1995;33(4):529–33.
[233] Sprinkart AM, Luetkens JA, Träber F, Doerner J, Gieseke J, Schnackenburg B, et al. Gradient spin echo (GraSE) imaging for fast myocardial T2 mapping. J Cardiovasc Magn Reson 2015;17(1). 12-.
[234] Traficante DD. Relaxation. Can T2, be longer than T1? Concepts Magn Reson 1991;3(3):171–7.
[235] Zur Y. Analysis of the multi-echo spin-echo pulse sequence. Concepts Magn Reson 2017;46(A):21402. https://doi.org/10.1002/cmr.a.21402.
[236] Stables LA, Kennan RP, Anderson AW, Gore JC. Density matrix simulations of the effects of J Coupling in Spin Echo and Fast Spin Echo Imaging. J Magn Reson 1997;140(2):305–14. 1999.
[237] Winkler ML, Ortendahl DA, Mills TC, Crooks LE, Sheldon PE, Kaufman L, et al. Characteristics of partial flip angle and gradient reversal MR imaging. Radiology 1988;166(1 I):17–26.